The primate cortical LFP exhibits multiple spectral and temporal gradients and widespread task dependence during visual short-term memory

Steven J. Hoffman, Nicholas M. Dotson, Vinicius Lima and Charles M. Gray

J Neurophysiol 132: 206–225, 2024.
First published June 6, 2024; doi:10.1152/jn.00264.2023

american physiological society

JNP JOURNAL OF NEUROPHYSIOLOGY

RESEARCH ARTICLE

Sensory Processing

The primate cortical LFP exhibits multiple spectral and temporal gradients and widespread task dependence during visual short-term memory

Steven J. Hoffman,[1,3] Nicholas M. Dotson,[1,4] Vinicius Lima,[2] and Charles M. Gray[1]

[1]*Department of Cell Biology and Neuroscience, Montana State University, Bozeman, Montana, United States;* [2]*Aix Marseille Université, INSERM, Systems Neuroscience Institute, Marseille, France;* [3]*Department of Biomedical Engineering, University of Minnesota, Minneapolis, Minnesota, United States; and* [4]*Salk Institute for Biological Studies, La Jolla, California, United States*

Abstract

Although cognitive functions are hypothesized to be mediated by synchronous neuronal interactions in multiple frequency bands among widely distributed cortical areas, we still lack a basic understanding of the distribution and task dependence of oscillatory activity across the cortical map. Here, we ask how the spectral and temporal properties of the local field potential (LFP) vary across the primate cerebral cortex, and how they are modulated during visual short-term memory. We measured the LFP from 55 cortical areas in two macaque monkeys while they performed a visual delayed match to sample task. Analysis of peak frequencies in the LFP power spectra reveals multiple discrete frequency bands between 3 and 80 Hz that differ between the two monkeys. The LFP power in each band, as well as the sample entropy, a measure of signal complexity, display distinct spatial gradients across the cortex, some of which correlate with reported spine counts in cortical pyramidal neurons. Cortical areas can be robustly decoded using a small number of spectral and temporal parameters, and significant task-dependent increases and decreases in spectral power occur in all cortical areas. These findings reveal pronounced, widespread, and spatially organized gradients in the spectral and temporal activity of cortical areas. Task-dependent changes in cortical activity are globally distributed, even for a simple cognitive task.

NEW & NOTEWORTHY We recorded extracellular electrophysiological signals from roughly the breadth and depth of a cortical hemisphere in nonhuman primates (NHPs) performing a visual memory task. Analyses of the band-limited local field potential (LFP) power displayed widespread, frequency-dependent cortical gradients in spectral power. Using a machine learning classifier, these features allowed robust cortical area decoding. Further task dependence in LFP power were found to be widespread, indicating large-scale gradients of LFP activity, and task-related activity.

cognition; electrophysiology; large-scale; LFP; short-term memory

INTRODUCTION

Extensive evidence, from studies in both humans and nonhuman primates, has established that cognitive tasks engage synchronized neuronal oscillations in multiple frequency bands among widely distributed cortical areas (1–13). A number of functional roles have been proposed for these cortical rhythms, ranging from perceptual binding (14, 15), working memory (7, 12, 16), and attention (17, 18) to inhibitory gating mechanisms (19, 20) and consciousness (21), often with the implicit assumption that the cortical rhythms of interest are expressed throughout the cortex. However, despite decades of research on the function and mechanisms of cortical oscillatory activity (22–25), it is still unclear how the various cortical rhythms are distributed across the cortical mantle.

Early electroencephalographic (EEG) recordings of human brain activity revealed salient oscillations in the α (~7–14 Hz) and β (~15–30 Hz) frequency bands (26–28). Spatial mapping of the surface cortical EEG revealed a wide distribution of α activity throughout parietal, temporal, and occipital regions, as well as portions of the anterior frontal lobe and more localized β activity in sensorimotor and premotor cortices (29). Recent magnetoencephalography (MEG) and intracranial EEG studies

Correspondence: S. J. Hoffman (hoff1695@umn.edu); C. M. Gray (cmgray.montana@gmail.com).
Submitted 10 July 2023 / Revised 17 May 2024 / Accepted 5 June 2024

have revealed distinct spectral features among the array of cortical areas (30, 31) and spatial gradients of peak frequency within the α and β bands (32). However, both approaches have significant limitations. Intracranial EEG recordings are limited in scope and the spatial resolution of MEG methods is hampered by the superposition of signals from multiple brain areas and the general dominance of the ongoing α rhythm (30). Therefore, a high-resolution map of cortical oscillatory activity has remained elusive.

Elucidating the spatial and task-dependent organization of cortical oscillatory activity is an especially timely question, given recent discoveries of anatomical and functional gradients underlying the hierarchical organization of cortex (33–36). Striking correlations have been established between gradients of dendritic spine counts (37, 38), cell density (39, 40), neurotransmitter receptor expression (41, 42), and the anatomical hierarchy defined by interareal connections (43–45). Measures of the intrinsic time scale of neural activity across cortical areas also display a hierarchical organization consistent with the underlying anatomy (46–52). However, these functional studies do not include, or even discard, the oscillatory components of the signals under consideration. Consequently, a large gap exists in our understanding of how these anatomical and functional gradients are organized in relation to cortical oscillatory activity and its task dependence.

To address these questions, we developed and utilized a novel microdrive system to measure intracortical neural activity from a total of 55 identified cortical areas in two macaque monkeys that were engaged in a visual short-term memory task (50, 53, 54). We measured both the power spectrum and the sample entropy (SampEn) (55, 56) of the local field potential (LFP) to identify the predominant frequency bands of oscillatory activity, the relative and absolute amplitude of the signals in each band, and the temporal complexity of activity in each of the measured areas. These metrics displayed unique spatial gradients across the cortical areas, some of which were correlated with excitatory synaptic spine counts obtained from previous anatomical studies (37, 38). Using the same metrics as features in a classifier, we found that cortical areas can be robustly decoded from each epoch of the task. All features and frequency bands contributed approximately equally to the classification performance. Task-dependent changes in spectral power occurred in all cortical areas and nearly in all frequency bands in both animals, revealing that even a simple cognitive task engages widespread areas of the cortical mantle (57).

METHODS

Detailed descriptions of the experimental methods for behavioral training, neural recording, and preprocessing of the data have been described in two previous reports (50, 54). We provide brief descriptions of these methods here.

All procedures were performed in accordance with NIH guidelines and approved by the Institutional Animal Care and Use Committee of Montana State University.

Behavioral Task

Two female macaque monkeys were trained to perform an object-based delayed match to sample task [dMTS; MonkeyLogic software (58, 59)]. A schematic illustrating the time course of events in the task is shown in Fig. 1*A*. A trial began when the animal acquired and fixated on a small white fixation spot displayed on a gray background [presample period; fixation window = 3 degrees of visual angle (dva)]. After 500 ms for *monkey E*, and 800 ms for *monkey L* the fixation dot was replaced with one of five randomly selected sample images for 500 ms (size: 2.4 × 2.4 dva). The five daily images used were drawn from a larger pool of 92 images. During the sample period, the monkey had to maintain its gaze within a 3° window encompassing the image. Next the sample image was extinguished and replaced with the fixation dot for a variable delay period (800–1,200 ms *monkey E*; 1,000–1,500 ms *monkey L*). At the end of the delay period, the fixation target was extinguished, and the matching image and a nonmatching image (one of the four other images) appeared at 5° from the center of the screen. For *monkey E*, the match and nonmatch images were always placed randomly in opposite hemifields along the horizontal axis. For *monkey L*, the images were randomly aligned either vertically, horizontally, or 45° diagonally across from each other (see Fig. 1*A*). Finally, while the match images were visible, the monkey had to make a saccadic eye movement to the matching image and maintain fixation for a brief period (200 ms for *monkey E*, and 500 ms for *monkey L*). Correct trials were rewarded with a drop of juice.

Electrophysiological Recording

Broadband recordings (0.1 Hz–9 kHz, sampled at 32 kHz) were made across the breadth of a cerebral hemisphere in the two monkeys as described in a study by Dotson et al. (54). Briefly, a hemisphere-wide, large-scale microdrive was implanted in two female macaque monkeys with the capability of simultaneously recording from up to 256 independently moveable microelectrodes (interelectrode spacing = 2.5 mm) (Fig. 1*B*). Neural activity was sampled from an overlapping set of 62 cortical areas over the course of 6 and 9 mo for *monkeys E* and *L*, respectively (Fig. 1*C*). The broadband signal was bandpass filtered at 1–250 Hz (4th-order Butterworth) and resampled at 1 kHz to obtain the LFP. Anatomical designations [using the nomenclature of Markov et al. (43)] were achieved through reconstruction of each electrode's track through histological sections (54). Only recordings with neural unit activity that exceeded a minimum mean firing rate of 1 Hz were used for further analysis. Spike waveforms were extracted by detecting local minima in the highpass signal (500 Hz–9 kHz) that exceeded 5 SDs of the noise level (7, 8, 50, 60). To avoid the oversampling of activity, only LFP signals where the electrode position differed from the previous day of recording by >250 μm in depth were used in this analysis.

Areal Grouping

Data from adjacent cortical areas with few recordings and similar functional properties were pooled to form small groups of areas. Recordings in visual areas V1 and V2 with short-latency visual responses in the unit activity (SLVR) were analyzed separately (i.e., V1-SLVR, V2-SLVR). The SLVR designation was assigned if the unit activity displayed a significant change in firing rate within 50–100 ms following the sample presentation. After these pooling procedures, there were a total of 29 and 34 different cortical areas or small groups of areas in *monkeys E* and *L*, respectively (Table 1).

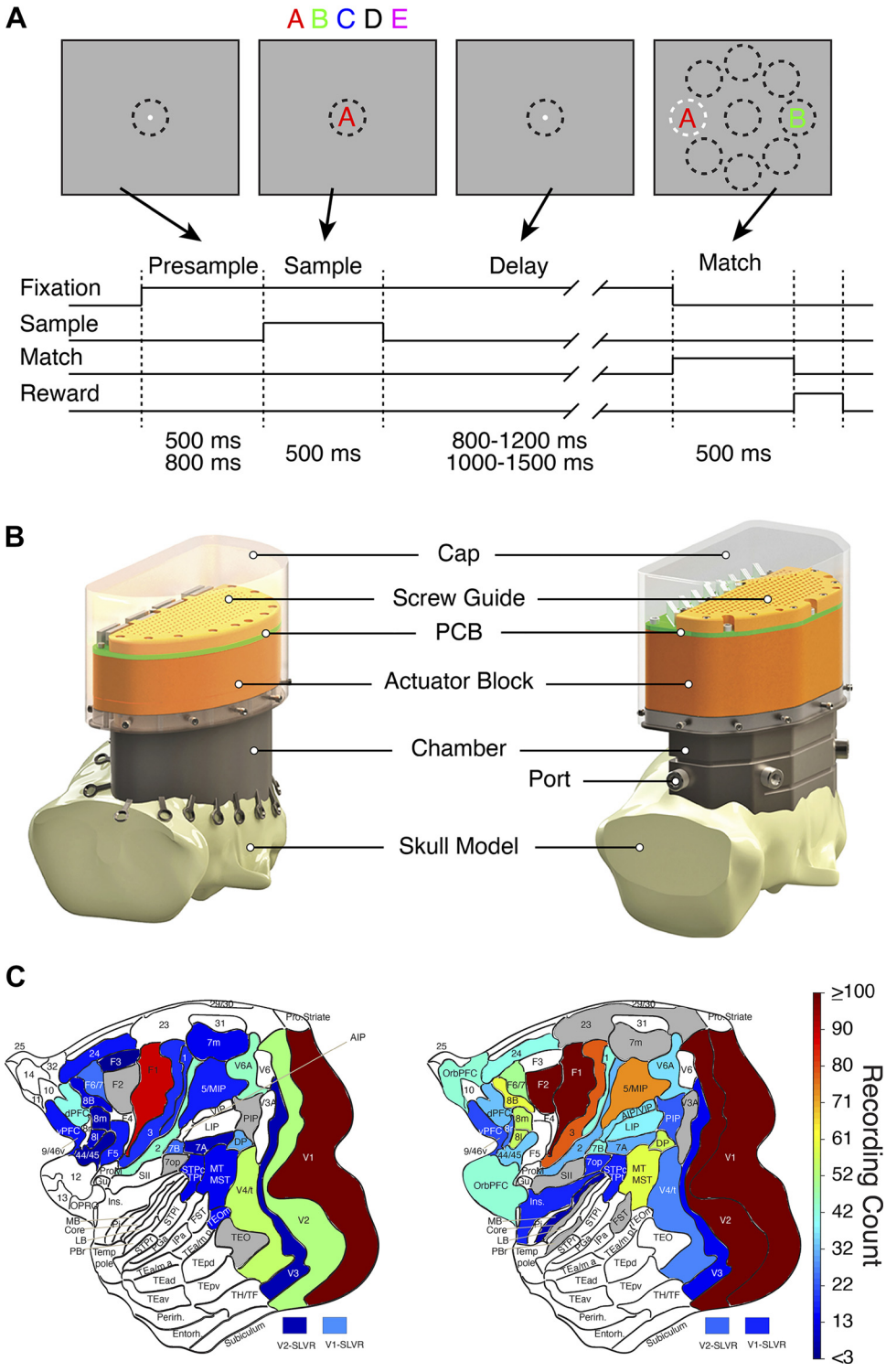

Figure 1. *A*: time course of events in the delayed match-to-sample task. The upper frames illustrate the sequence of images viewed by the monkeys during the task. The dashed circles represent the windows for monitoring eye position. These were not visible to the animal. The sample and match stimuli are symbolized by the letters A–E. The white dashed circle in the right plot indicates a correct match. The lower plot illustrates the timeline of task events. The presample duration was 500 ms for *monkey E* and 800 ms for *monkey L*. The duration of the delay period was 800–1,200 ms for *monkey E* and 1,000–1,500 ms for *monkey L*. Match stimuli were randomly presented on opposite sides of the horizontal for *monkey E* and on opposite sides of axes lying at 0, 45, and 90 degrees for *monkey L*. *B*: design drawings of the chamber and semi-chronic microdrive systems used for recording neuronal activity. The left and right designs were used on *monkeys E* and *L*, respectively. Adapted from Dotson et al. (54). *C*: flatmaps of the recording counts for each cortical area/group [following the nomenclature of Markov et al. (43)] in *monkeys E* (*left*) and *L* (*right*). Areas with less than three recordings are shaded gray and were not included in the analyses. Areal groupings and recording counts are listed in Table 1.

Identification of Spectral Bands

For each recording, the power spectral density, averaged across all correct trials in a session, was calculated from 1 to 100 Hz [Field Trip toolbox (61)]. A multi-taper smoothing window of 1 Hz was used. In *monkey E*, residual 60 Hz line noise was removed with a notch filter. Spectra were calculated over a time window of 2,100 ms encompassing the task period from presample until match onset. Due to the variable length of the delay period, trials that were less than 2,100 ms in length were zero padded to achieve this length. Longer trials were truncated to fit the 2,100 ms time window. The frequency resolution of the power spectra was 0.5 Hz.

We used an empirical method to designate the frequency band limits for further analysis. We applied a peak detection algorithm (findpeaks.m in Matlab) to the normalized power spectra from 4–100 Hz, in both linear and semi-log coordinates, to identify narrow band oscillatory activity. Local

Table 1. *Recording counts for all areas and areal groupings in monkeys E and L*

		Monkey E		Monkey L	
Areas	Area/Group	Flatmaps	Decoding	Flatmaps	Decoding
OPRO, 11,12,13,14,32	OrbPFC			42	42
24c, 24d	a24	14		40	40
9/46v, 46v	vPFC	14		20	20
9/46d, 9, 46d	dPFC	40	40	32	32
8B	8B	10		60	60
8L	8L	9		55	55
8M	8M	6		54	54
8r	8r			25	25
44, 45 A, 45B	a44/45	5		33	33
F1	F1	90	90	102	102
F2	F2			120	120
F3	F3	3			
F5	F5	15			
F6, F7	F6/F7	24	24	49	49
1	1	17		41	41
2	2	43	43	31	31
3	3	17		79	79
Insula	Ins			16	
MB	MB			6	
7op	7op			16	
7m	7m	12			
a5, MIP	a5/MIP	15		74	74
PIP	PIP			22	22
7a	7a	7		30	30
STPc, TPt	STPc/TPt	12		15	
AIP, VIP	AIP/VIP			35	35
7b	7b	23	23	41	41
LIP	LIP			37	37
DP	DP	30	30	56	56
V6A	V6A	44	44	35	35
MT, MST	MT/MST	12		59	59
TEOm	TEOm	13			
V4, V4t	V4/t	54	54	26	26
V3	V3	6		12	
V2SLVR	V2SLVR	6		23	23
V2	V2	51	51	117	117
V1SLVR	V1SLVR	27	27	16	
V1	V1	169	169	225	225
Recording count		788	526	1,644	1,563
Area/groups		29	11	34	28

Area and areal group names are given in the first and second columns, respectively. Columns labeled as "Flatmaps" show the recording counts reported in flatmaps and rank ordered plots of spectral content (SC), peak amplitude (PA), and sample entropy (SampEn). Columns labeled as "Decoding" show the area/groups that are included in the classification analysis.

maxima <4 Hz were excluded, due to artifactual peaks introduced by the multi-taper smoothing filter. To limit small, spurious peaks, a peak prominence criterion (as defined by the Matlab findpeaks.m function) was used. The prominence threshold was set at 1% of the maximum prominence found across all spectra. Values exceeding the prominence threshold were used to generate a histogram of peak frequencies across all recordings in each animal. The histograms were fit with a probability density function (PDF) using a mixture of Gaussians (Fitdist.m function in Matlab). Frequency band limits were designated as the local minima in the PDFs. This analysis yielded nearly identical band limits when applied to the linear and semi-log spectra, with deviations in frequency bands being less than 1.5 Hz. Results from the two approaches were combined by averaging the local minima designations from the two methods.

Classifier Features

We first computed the average power spectral density (1-Hz multi-taper smoothing window) across all trials for each of five 400-ms epochs of the task (see Fig. 2*B*) on each recording [Field Trip toolbox (61)]. Using the band limits defined for each monkey, we measured the spectral content (SC) and the peak amplitude (PA) of the spectrum in each frequency band and epoch of the task for the entire data set in each animal. We defined SC as the percentage of power within each frequency band relative to the entire spectrum (0–80 Hz) and PA as the largest value of the average spectrum in each band.

To quantify the complexity, or degree of randomness, of the LFP, we calculated the sample entropy [SampEn (m, r, N)] on each task epoch of each trial for each recording (55). We used the average value of SampEn across trials for each epoch as a feature. SampEn is an event counting statistic, derived from approximate entropy (ApEn) (62), which quantifies the persistence or regularity of similar patterns in a signal. It is defined as "the negative natural logarithm of the conditional probability that two sequences similar for m points remain similar at the next point, where self-matches are not included in calculating the probability" (55,

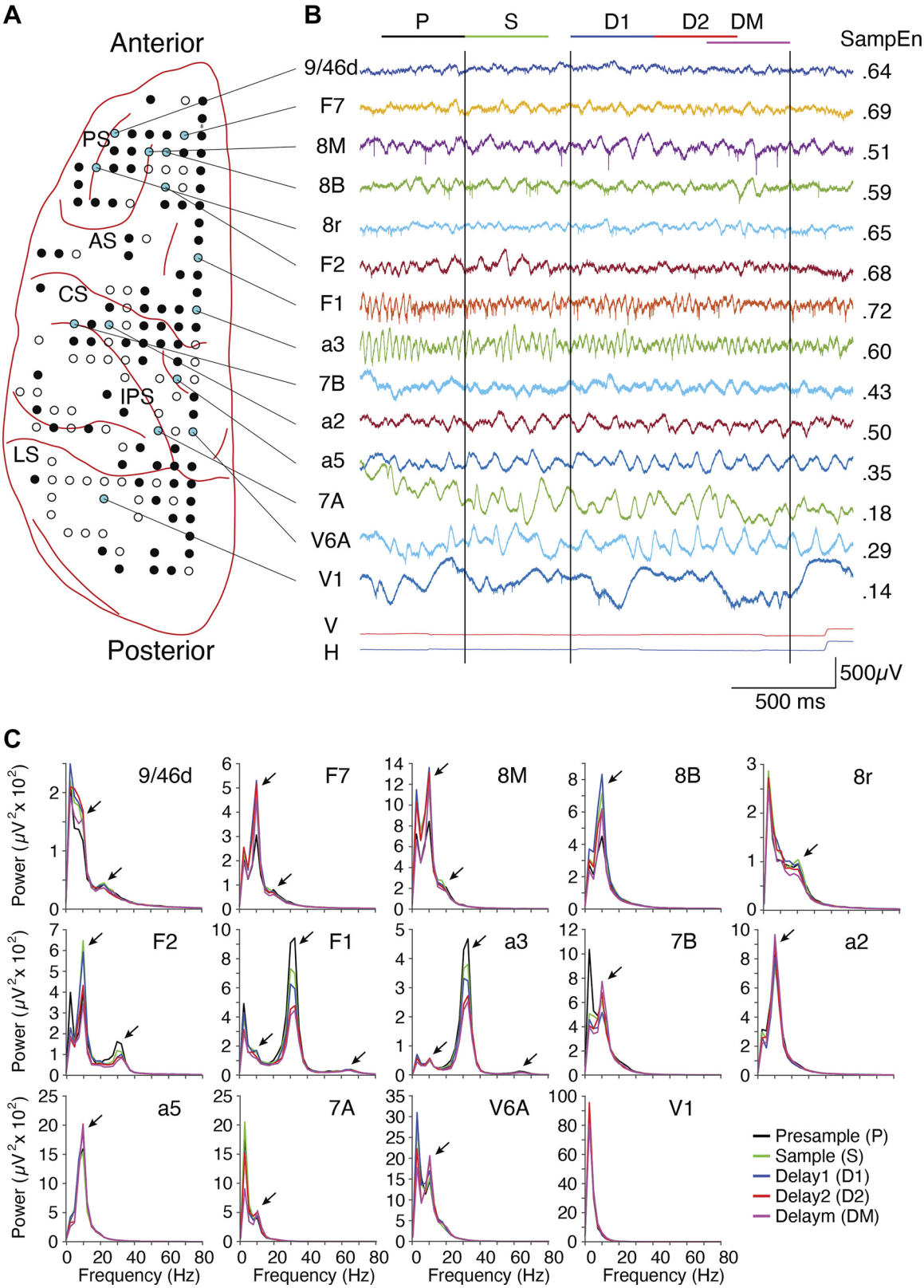

56). It reduces the bias associated with ApEn and is largely independent of the record length of the data:

$$\mathrm{SampEn}(m, r, N) = -\ln\left[A^m(r)/B^m(r)\right]$$

where

$B^m(r)$ is the probability that two sequences are similar for m points (possibles)

$A^m(r)$ is the probability that two sequences are similar for $m + 1$ points (matches)m is the length of the sequences being compared$r$ is the threshold for accepted matches, expressed as a fraction of the standard deviation (σ) of the time series$N$ is the length of the time series being evaluated.

We used values of $m = 2$ and $r = 0.2\sigma$. $N = 400$ data points, which is the length of each task epoch. Each data epoch of length N was z-score normalized before computing SampEn.

Together, these analyses resulted in nine features in each of five epochs in *monkey E* (SC and PA in *bands 1–4*, and SampEn) and 11 features in each of five epochs in *monkey L* (SC and PA in *bands 1–5*, and SampEn).

Machine Learning Classifier

Each of the features were included in a cubic support vector machine (SVM) classifier. Cortical areas with small numbers of recordings were grouped with those in adjacent areas with similar functional properties (Table 1). To avoid bias (in both the training and validation phases) toward areas with substantially more recordings, an equal number of recordings ($n = 20$) from each area/group were randomly drawn from the larger pool of data. The classifier was trained and validated using k-fold cross validation ($k = 5$, 4/5th training, 1/5th cross validation). The training-validation process was iteratively repeated 1,000 times, with each iteration using a different set of 20 randomly selected recordings for an area/group drawn from the data pool (Table 1). The theoretical level of chance classification is 1/no. of areas (1/11 *monkey E*, 1/28 *monkey L*). To further assess classification accuracy and avoid biases arising from the use of the theoretical chance level (63), the mean and 99% confidence interval for chance classification was calculated from a permutation distribution. This distribution was created by randomly shuffling areal/group labels before the classification process, then repeating over 1,000 iterations.

RESULTS

We recorded broadband neuronal activity from a total of 55 cortical areas in two rhesus macaque monkeys (33 areas in *monkey E* and 50 areas in *monkey L)* while they performed a feature-based delayed match-to-sample (dMTS) task and an interleaved visual fixation task (Fig. 1*A*). The dMTS task required the monkeys to remember a centrally presented sample image (1 of 5 possible images) for a minimum of 800 ms (800–1,200 ms in *monkey E*; 1,000–1,500 ms in *monkey L*), before making a choice between a matching and a nonmatching image. Details of the recording methods, the behavioral task, reconstruction of the recording sites, and analysis of the task dependence of unit activity have been reported previously (50, 54). Here, we focus on the spatial and spectro-temporal organization of the LFP and its task dependence. LFP signals were selected for analysis only if there was detectable unit activity recorded on the same electrode, and if the electrode position had changed by more than 250 μm from the previous session of recording, yielding a unique recording site. LFP signals that were noisy or had frequent artifacts were discarded, following the methods described by Salazar et al. (7). All analyses were performed on the correct trials of the dMTS task, obtained from 25 sessions in *monkey E* and 61 sessions in *monkey L* (minimum 500 correct trials and >75% correct performance on each session). Simultaneous recordings were made from up to 21 and 37 different cortical areas in *monkeys E* and *L*, respectively. The cortical area of the recording locations and sample sizes for each animal are shown in Fig. 1*C* and Table 1. Data from sparsely sampled and adjacent cortical areas with similar functional properties were merged into small groups. This resulted in a total of 788 recordings from 33 areas merged into 29 area/groups in *monkey E* and a total of 1,644 recordings from 50 areas merged into 34 area/groups in *monkey L* (Table 1). For simplicity, we use the term "areas" throughout the text when describing our findings for cortical areas and small groups of areas.

Spatial Organization of the LFP

At the outset of these experiments, it was apparent that the spectral and temporal properties of the LFP varied systematically across the cortex in a task-dependent manner. Figure 2 shows a representative example of the raw data, and corresponding LFP power spectra, sampled from a subset of the channels on a single session in *monkey L*. Prefrontal (9/46d), frontal eye field (8M, 8B, 8r), and premotor (F7, F2) areas tended to display desynchronized fluctuations of low amplitude interspersed with brief intervals of periodic activity in the range of 6–14 Hz. Primary motor and somatosensory areas, F1 and a3, exhibited pronounced oscillations in the 25–35 Hz range, that occurred with lower amplitude in premotor areas. Anterior (a2, a5, 7B) and posterior (7A, V6A)

Figure 2. Spectral properties of local field potential (LFP) signals vary markedly across cortex. *A*: schematic of the recording sites in *monkey L*. The outline of the left hemisphere and major cortical sulci, drawn from a photograph, are shown in red. Each circle shows the entry location of an electrode that recorded neural unit activity at some point during the 9 mo of the experiment. Filled circles indicate electrode locations that recorded neural activity in this session ($n = 94$). Cyan-filled circles mark the electrode locations that correspond to the signals shown in *B*. *B*: broadband (0.1 Hz–9 kHz) raw data recorded on a single trial from 14 separate cortical areas. The areal name (left of each trace) follows the nomenclature of Markov et al. (43). The bottom two traces show the vertical and horizontal components of the eye position signal. The black vertical lines, from left to right, mark the onset and offset of the sample stimulus and the onset of the match stimulus, respectively. The colored horizontal bars at the top indicate the time and duration (400 ms) of the Presample (P), Sample (S), Delay1 (D1), Delay2 (D2), and DelayM (DM) epochs, respectively. A saccadic eye movement, occurring ~200 ms following the onset of the match, indicates the monkey's behavioral choice. The mean sample entropy (SampEn) across trials is plotted to the right of each data trace. *C*: LFP power spectra (0–80 Hz) for each area indicated in *A* and *B*, averaged across all correct trials for each of the five epochs (Presample: black; Sample: green; Delay1: blue; Delay2: red; Delaym: magenta). Clear differences in LFP power and its task dependence are apparent between different areas of cortex. Black arrows mark notable local peaks or shoulders in the power spectra. Peaks occurring below 4 Hz are due to the absence of a DC component in the filtered signals. AS, arcuate sulcus; CS, central sulcus; IPS, intraparietal sulcus; LS, lunate sulcus; PS, principal sulcus.

parietal areas exhibited higher amplitude fluctuations with salient oscillations in the 6–14 Hz range. Primary visual cortex (V1) was dominated by high amplitude fluctuations at low frequencies. Each of these aspects were clearly apparent in the corresponding power spectra (Fig. 2*C*), which were computed from five separate 400-ms epochs of the task [presample (P), sample (S), early delay (D1), late delay (D2), match locked delay (DM), Fig. 2*B*]. There were notable peaks in the spectra that often varied between task epochs. Some spectra showed a sharp singular peak centered around 10 Hz (Fig. 2*C*, areas 8B, 7B, a2, a5, 7A, V6A), whereas others displayed multiple peaks around 10 Hz and 30 Hz (Fig. 2*C*, areas F2, F1, a3), and in some cases small peaks near 65 Hz (Fig. 2*C*, areas F1, a3). Smaller peaks and shoulders were also apparent near 20 Hz (Fig. 2*C*, areas 9/46d, F7, 8M, 8r). Other recordings, most notably in early visual cortex, displayed a steep fall off in power, with very low amplitudes at higher frequencies (Fig. 2*C*, area V1).

To determine the appropriate frequency bands for subsequent analysis, we identified local peaks in the average power spectra, in both linear and semi-log coordinates, computed across all correct trials over the full trial length for all recordings in both animals (Supplemental Figs. S1 and S2). This analysis yielded a histogram of peak frequencies, and their corresponding areas of origin, spanning the full data set in each monkey (Fig. 3). The histograms derived from the linear and semi-log spectra were nearly indistinguishable and had no effect on the selection of frequency bands (Supplemental Fig. S3). Frequencies below 4 Hz were excluded to avoid the detection of spurious peaks due to filtering. We fit each histogram with a probability density function (PDF) and found the local minima in the distributions. This resulted in four frequency bands in *monkey E* (0–8 Hz, 8–21 Hz, 21–32 Hz, 32–80 Hz) and five bands in *monkey L* (0–6 Hz, 6–14 Hz, 14–26 Hz, 26–42 Hz, 42–80 Hz). These bands did not change after removing the data from all areas that were not present in both animals (V1SL in *monkey E* and OrbPFC, 8r, Ins, AIP/VIP, LIP in *monkey L*).

These data revealed a notable difference in the frequency distribution of narrow-band oscillations between the two monkeys. Low-frequency spectral peaks (*band 1*) were sparsely distributed in both monkeys. Spectral peaks in *band 2*, centered at 14 Hz in *monkey E* and 10 Hz in *monkey L*, were widely distributed and present in nearly all areas of cortex. Peak frequencies in *band 3* were centered at 25 Hz in *monkey E* and 21 Hz in *monkey L* and were frontally distributed. There were more obvious differences between the animals at higher frequencies. Spectral peaks in *band 4* were very sparse in *monkey E*, whereas monkey L showed pronounced narrow-band components in two bands (*band 4*, *band 5*) that were concentrated in somatomotor regions and some areas of the prefrontal and parietal cortices. The spectral peaks in *band 5* of *monkey L* were notable in that, with one exception, they always co-occurred with and had twice the frequency of the peaks in *band 4*. This suggested the presence of a higher frequency harmonic known to result from the nonsinusoidal nature of oscillations in LFP, EEG, and MEG signals (64–68). Detailed analysis of the *band 5* component, in both the frequency and time domains (see Frequency Harmonic Analysis in Supplemental Materials), confirmed this conjecture (Supplemental Figs. S4, S5, S6, and S7). Some high-frequency components were also sparsely present in early visual cortex in both animals, consistent with the occurrence of induced γ-band activity in response to the sample stimuli (69). Many areas displayed a unimodal distribution, whereas other areas showed bimodal

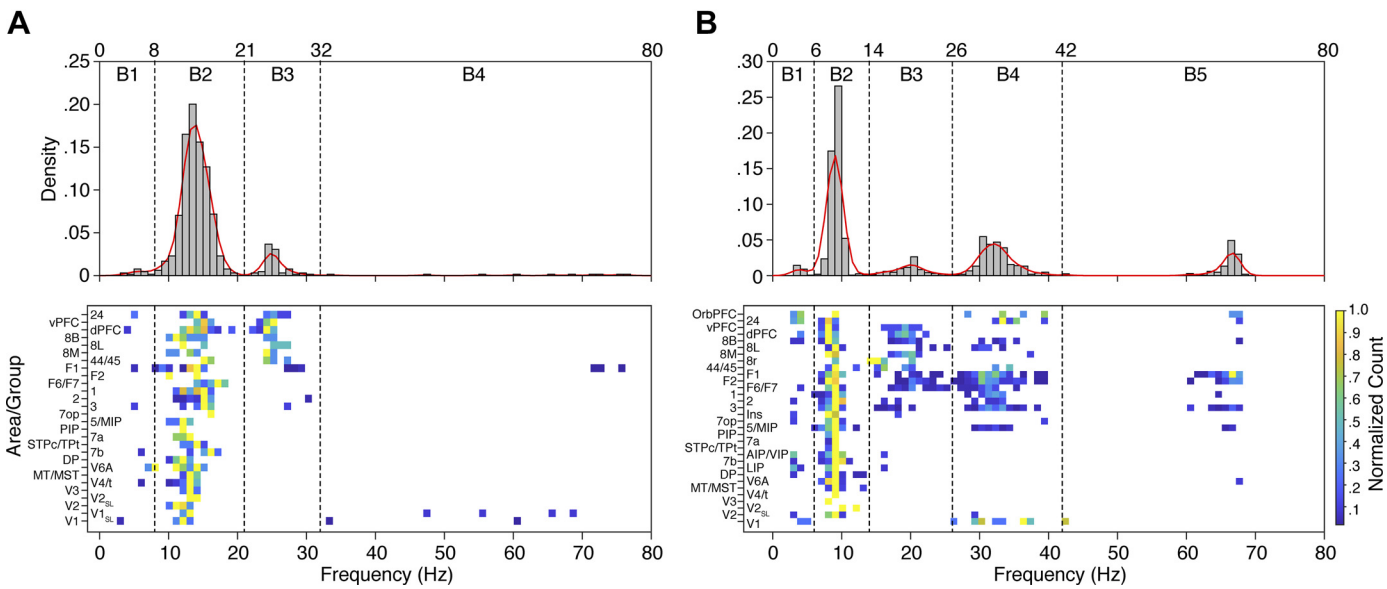

Figure 3. Spectral peaks in the local field potential (LFP) occur in distinct frequency bands that vary between animals. Distributions of peak frequencies obtained from semi-log power spectra on all channels and sessions in *monkeys E* (*A*) and *L* (*B*). The *top* plots in *A* and *B* show the cumulative histograms of all peak frequencies (4–80 Hz) that exceeded the peak prominence threshold (see Supplemental Figs. S1 and S2). The continuous red lines show the probability density function (PDF) computed with a mixture of Gaussians fit to each distribution. The local minima in each PDF define the boundaries between selected frequency bands for each animal (dashed vertical lines). Four bands (*B1–B4*) were chosen for *monkey E* and five bands (*B1–B5*) were chosen for *monkey L*. The *bottom* plots show the normalized counts of peak frequencies for each cortical area/group. This revealed a rough spatial organization of peak frequencies across the sampled cortical areas.

or even multimodal distributions of spectral peaks. This was most evident in *monkey L*. These results reveal distinct differences between animals in the frequency composition of narrow band oscillations in the cortical LFP.

To determine if cortical areas can be distinguished by the spectral properties of their LFP, we extracted two values from the spectra computed on each epoch: the percentage of power in each frequency band relative to the entire spectrum (0–80 Hz), which we refer to as the spectral content (SC), and the peak amplitude (PA) of the power in each band. The PA was distinct from SC because it reflected the absolute amplitude of the signals, which varied widely across cortical areas, and was not bounded within a range of 0–100% (Fig. 2*C*). To assess the spatial organization of spectral power across the cortex, we plotted the mean value of SC in the presample epoch (across sessions) on cortical flatmaps (adapted from Ref. 43) for each frequency band (Fig. 4). The corresponding rank-ordered box plot of SC (sorted on the median value) is displayed to the right of each flatmap to visualize the distribution of values across cortical areas. These maps revealed striking spatial gradients of SC that differ between frequency bands and display similarities as well as differences between the two animals. In both monkeys, there was a clear posterior to anterior gradient of SC in *band 1*, with the greatest concentration of power occurring in visual cortices. *Band 2* displayed an anterior shift in the distribution with relative power radiating out from more central/parietal regions. In the higher frequency bands [3 and 4 in *monkey E* (Fig. 4*A*), 3–5 in *monkey L* (Fig. 4*B*)] there was an anterior shift in the distribution of SC with increasing frequency. A notable difference between animals was also present in the higher frequency bands. *Monkey L* displayed a distinct focal distribution of high amplitude (*band 4*) in somatomotor areas (3, F1, and F2) with a declining gradient into premotor, prefrontal, and anterior parietal areas that was not present in *monkey E*. Similar plots of PA are shown for both monkeys in Fig. 5. These data reveal pronounced amplitude differences across areas within each band as well as striking differences in the LFP amplitude between different frequency bands. The spatial gradients are also apparent, but more variable than those shown by the normalized measure of SC in Fig. 4.

The LFP also displayed marked variation in temporal structure across different areas of cortex (Fig. 2*B*). To quantify this, we computed the sample entropy (SampEn) of each LFP time series (55, 56) (see METHODS). SampEn is an event counting statistic, derived from approximate entropy (ApEn) (62), which quantifies the persistence or regularity of similar patterns in a signal. It reflects the degree of a signal's randomness or complexity. A low value of SampEn indicates more self-similarity in a time series of LFP data. For each channel on each session, we calculated the average SampEn across trials on each epoch of the task. Examples of the mean SampEn values, averaged across epochs, are plotted to the right of the data traces in Fig. 2*B*. SampEn was lower in posterior occipital and parietal areas and increased in somatomotor and prefrontal areas. This effect was consistent with the data as a whole. Flatmaps and corresponding rank-ordered box plots of SampEn (presample epoch) for the full data set are shown for both monkeys in Fig. 6. This revealed a clear spatial gradient of SampEn from occipital to prefrontal regions of the cortex.

The organization of the LFP gradients suggested they may be related to the well-documented variation of synaptic spine counts on the basal dendrites of layer 3 pyramidal neurons (37), which exhibit a striking correlation to anatomical hierarchy (36, 44, 45). To test this conjecture, we computed the correlation between the published values of mean spine counts (38, 70–75) and the median values of SC, SampEn, and PA in each band in each monkey for all the cortical areas in which these data were available (Table 2). The distribution of average dendritic spine counts from a closely overlapping set of 14 areas in *monkey E* and 18 areas in *monkey L* were correlated with the spectral content and peak amplitude in *band 1* (SC1, PA1) and SampEn in both monkeys. Scatter plots and corresponding correlation coefficients (computed from all values in both monkeys) for these parameters are shown in Fig. 7. The low-frequency spectral components (SC1, PA1) were negatively correlated with mean spine count whereas SampEn displayed a positive correlation. Significant correlations were also present in higher frequency bands in *monkey L* (SC2, SC3, SC5, and PA2) but not in *monkey E* (Table 2).

Decoding Cortical Areas

Having identified a set of features that reveal spatial gradients of the spectral and temporal properties of the LFP, we sought to determine if these features could be used to classify cortical areas. We used a support vector machine (SVM) classifier algorithm, using a *K*-fold cross validation scheme ($K = 5$), and applied it separately to the full data set from each monkey, on each epoch of the task (see METHODS). Data were included in the analysis if each area contained a minimum of 20 recordings (resulting in 11 areas for *monkey E* and 28 areas for *monkey L*; Table 1). The analysis included nine features for *monkey E* (SC and PA in 4 frequency bands, and SampEn) and 11 features for *monkey L* (SC and PA in 5 frequency bands, and SampEn). The results of the classification analysis are shown in Fig. 8. The confusion matrices (Fig. 8, *A* and *B*), and corresponding distributions of validation accuracies (VA) (Fig. 8, *C* and *D*), are shown for the presample epoch in *monkey E* (Fig. 8, *A* and *C*) and *monkey L* (Fig. 8, *B* and *D*). The median values ranged from 35% to 85% in *monkey E* (Fig. 8, *A* and *C*) and 20% to 75% in *monkey L* (Fig. 8, *B* and *D*) and all areas exceeded the 99% confidence limit, computed from the permutation test (red lines in Fig. 8, *C* and *D*, see METHODS). As suggested by the gradients of SC, PA, and SampEn, classification errors tended to lie near the diagonal, indicating similarity in the spectral and temporal properties of the LFP among nearby areas within a cortical region.

To determine if VA was task-dependent, we compared the distributions in each area across the five epochs of the task. Figure 8, *E* and *F* shows the median VA in each area as a function of task epoch in *monkeys E* and *L*, respectively. These are the median values along the diagonals of the confusion matrices computed on each epoch. The corresponding distributions of VA are shown in Fig. 9. Task-dependent changes in VA were apparent in every area in both monkeys. In some areas VA increased during the delay period (e.g., DP and V2 in *monkey E*; 7b and V6A in *monkey L*), other areas displayed the opposite pattern (a2 in *monkey E*; a1 and a2 in *monkey L*), and many others displayed differences between

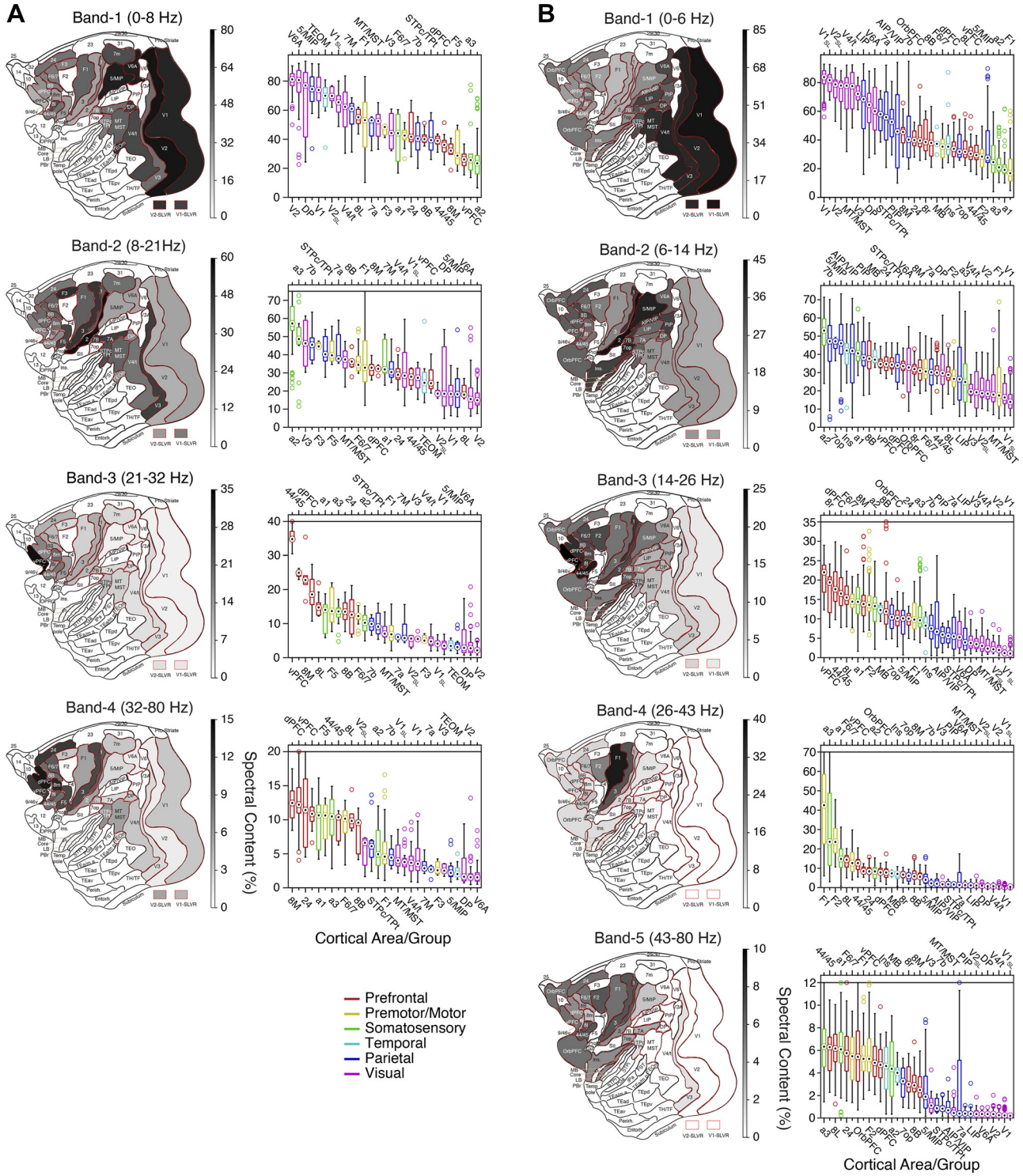

Figure 4. Spectral content displays anatomical gradients that differ across frequency bands in both monkeys (*A*: *monkey E*; *B*: *monkey L*). The left columns in *A* and *B* show cortical flatmaps of the mean spectral content in each area/group, across all sessions, during the presample epoch for each frequency band. Areal boundaries and nomenclature follow that of Markov et al. (43). Visual area V1 with short-latency visual responses in the unit activity (V1-SLVR) and visual area V2 with short-latency visual responses in the unit activity (V2-SLVR) refer to the subset of recordings in areas V1 and V2, respectively, that displayed short latency responses of spiking activity to one or more of the sample stimuli presented on each session [Dotson et al. (50)]. The right columns in *A* and *B* show the corresponding distributions of spectral content across all sessions, ranked by the median values. The circle within each box shows the median, the box displays the interquartile range, the whiskers show the 5th and 95th percentiles, and the open circles show outliers. Areal labels are displayed at the bottom and top of each plot. The data are color-coded by cortical region (prefrontal: red; premotor/motor: yellow; somatosensory: green; temporal: cyan; parietal: blue; visual: magenta).

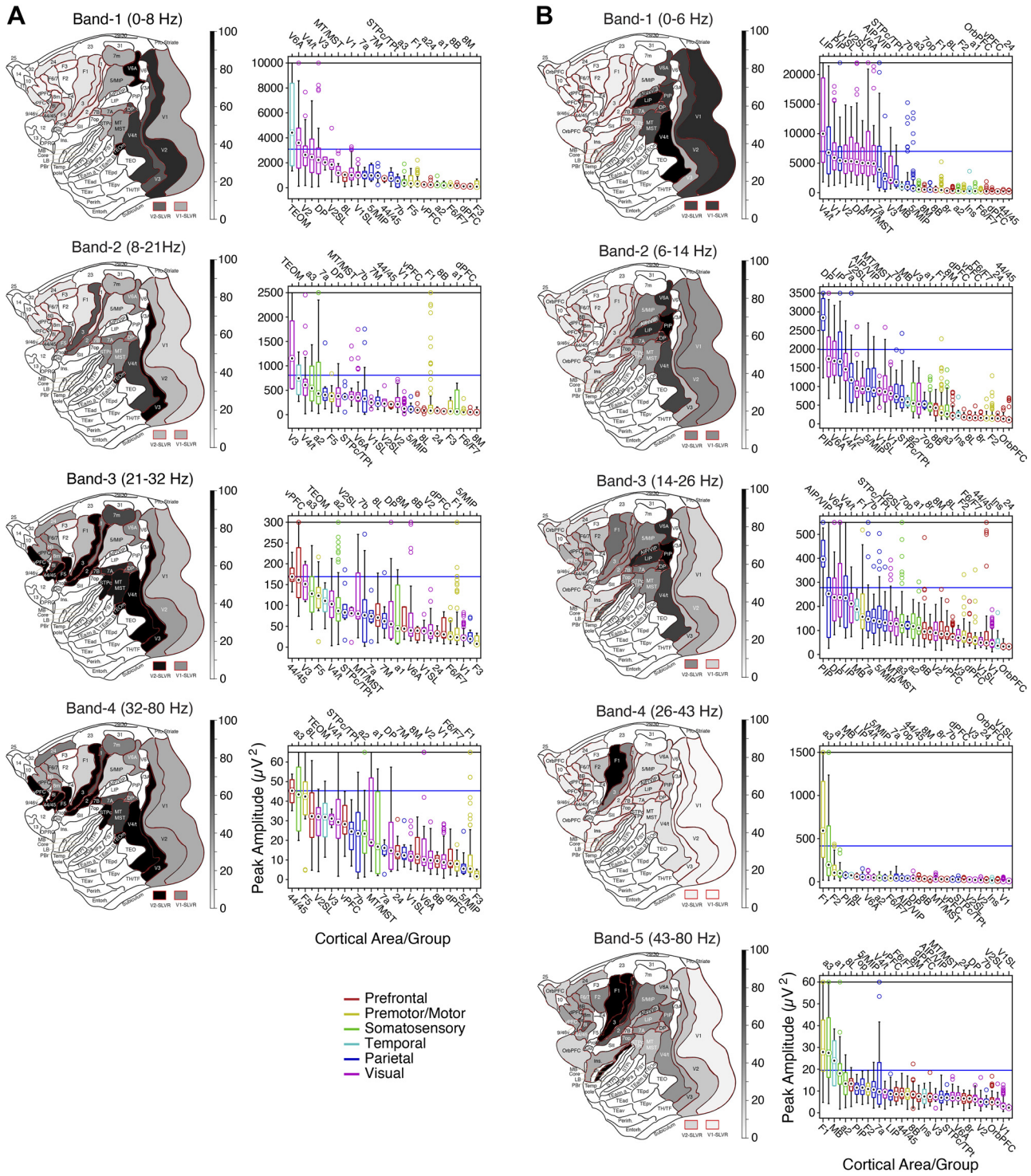

Figure 5. Flatmaps and rank-ordered box plots of the peak amplitude (PA) obtained from the power spectra in each frequency band in *monkey E* (*A*) and *monkey L* (*B*) during the presample epoch of the task. Plotting conventions are the same as Fig. 4. Because of outliers and nonlinearities in the rank order plots, the flatmaps are scaled as a percentage of a threshold value shown by the blue line in each rank ordered plot.

epochs with no discernible pattern across areas. In fact, every area examined in each animal showed a significant difference in VA across epochs (Kruskal–Wallis test, $P << 10^{-5}$, FDR corrected), suggesting widespread changes in the spectral and temporal properties of the LFP during the task that span all the cortical areas measured.

We performed several additional analyses to determine which features in the classifier were responsible for successful classification (see Feature Importance in Supplemental Materials). We first assessed the change in VA that occurs when the values of each feature are separately randomized. This led to a ~5% decrease in the mean VA across areas for

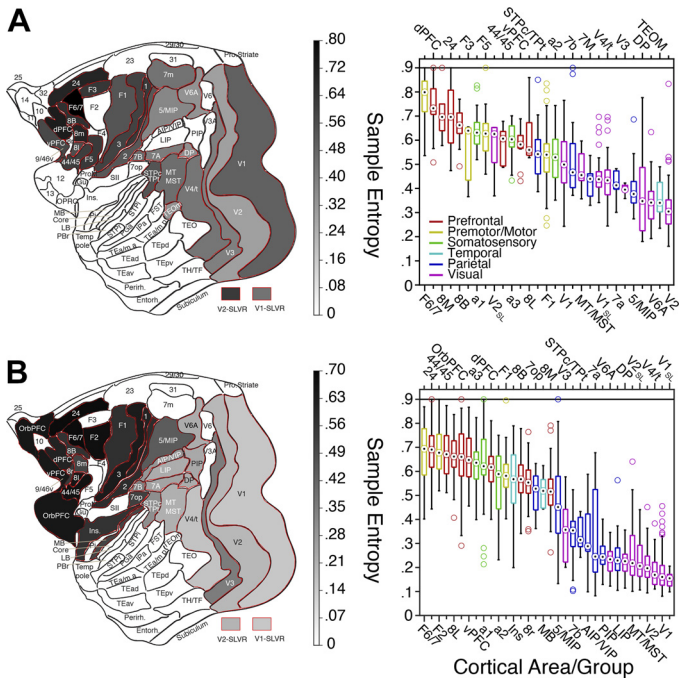

Figure 6. Sample entropy shows clear anatomical gradients. Variation of sample entropy (SampEn) across the cortex for both monkeys during the presample epoch. Cortical flatmaps of median SampEn (*left*) and corresponding distributions of SampEn, ranked by the median, for *monkeys E* (*A*) and *L* (*B*). Plotting conventions are the same as in Fig. 3.

each feature in both monkeys as compared with the baseline (Supplemental Fig. S8). We ran two additional analyses, after excluding SampEn as a feature. We assessed VA independently for SC and PA using the corresponding features in all frequency bands and we assessed the effect on VA of removing both features in each frequency band separately (Supplemental Tables S1 and S2). In both analyses, we found widespread, and often weak, effects that occurred in nearly all areas. We conclude that each feature makes a small contribution to validation accuracy and that no frequency band was substantially more informative than another.

We also sought to determine which features of the spectra account for classification errors between areas (see Areal Misclassification in Supplemental Materials). We found an inverse relation between VA and the variance of SC and PA in low frequency bands (SC1, SC2, PA1, PA2 in *monkey E*; SC1, SC2, PA1 in *monkey L*) (Supplemental Table S3) and a greater incidence of classification errors among nearby areas (Supplemental Fig. S9). Thus, both high variance in spectral features as well as similarity in feature values between nearby areas reduced validation accuracy. The latter result is consistent with our finding of spatial gradients in the spectral and temporal features of the LFP.

Task-Dependent Changes in Power

Although the classification analysis reveals widespread task-dependent changes in the cortical LFP, it does not provide a direct measure of the incidence, magnitude, or sign of those changes for each cortical area. We therefore performed a separate analysis of the change in spectral power across task epochs and frequency bands for each recording in the data set used for the classification analysis (11 areas in *monkey E*, 28 areas in *monkey L*). To screen out signals with low amplitudes, the mean spectral content in each band and epoch had to exceed 5%. For each trial in a session, we calculated the mean power within each band and each epoch. We compared the distribution of values across trials in the presample epoch to the distributions in each of the other four epochs using the Wilcoxon signed-rank test ($P < 0.01$, FDR corrected). This was repeated for every recording in an area resulting in a distribution of significant changes in power (both increases and decreases) occurring in each epoch and frequency band relative to the presample period (Fig. 10). Example results are shown in Fig. 10*A* [area 8B (*band 2*) and area F2 (*band 4*) in *monkey L*]. The mean of each distribution (black filled circle) and the incidence of significant differences (black horizontal line) are color coded and replotted in the lower two plots (see color scale in Fig. 10, *C* and *D*). In these examples, there was a mixture of power increases and decreases in *band 2* of area 8B that vary with task epoch, while the power in *band 4* of area F2 shows a sustained and increasing suppression throughout the task epochs (note that the incidence of significant suppression in area F2 exceeds 90% in each epoch). The overall incidence of changes in power, across all areas, epochs, and frequency bands, is shown for both monkeys in Fig. 10*B* (left plot: *monkey E*; right plot: *monkey L*). Significant changes in LFP power, relative to the presample period, occurred in 60% and 50% of the epochs in *monkeys E* and *L*, respectively. Decreases in power occurred nearly twice as often as increases in both monkeys.

To visualize the overall spatial pattern of these changes, we plotted the mean change in power and the incidence of occurrence in all epochs and frequency bands for all areas in

Table 2. *Correlation coefficients, and corresponding P values, between the median value of each spectral parameter in each frequency band and mean spine count of the basal dendrites of layer 3 pyramidal neurons in an overlapping set of 14 areas in monkey E and 18 areas in monkey L*

Monkey E	**SC1**	**SC2**	**SC3**	**SC4**		**SampEn**	**PA1**	**PA2**	**PA3**	**PA4**	
Correlation	−0.55	0.36	0.44	0.51		0.54	−0.59	−0.27	−0.1	−0.06	
P value	<0.05	<0.21	<0.12	<0.06		<0.05	<0.03	<0.35	<0.74	<0.85	
Monkey L	**SC1**	**SC2**	**SC3**	**SC4**	**SC5**	**SampEn**	**PA1**	**PA2**	**PA3**	**PA4**	**PA5**
Correlation	−0.64	0.6	0.73	0.21	0.51	0.68	−0.71	−0.62	−0.39	−0.04	−0.1
P value	<0.005	<0.009	<0.0007	<0.4	<0.03	<0.002	<0.0009	<0.006	<0.12	<0.89	<0.69

Adapted from Elston and Rosa (70–72); Elston and Rockland (73); Elston et al. (38, 74, 75). Spectral parameters are derived from the presample epoch of the task. Numerical values 1–5 indicate the separate frequency bands for each monkey. Significant values are highlighted in boldface.

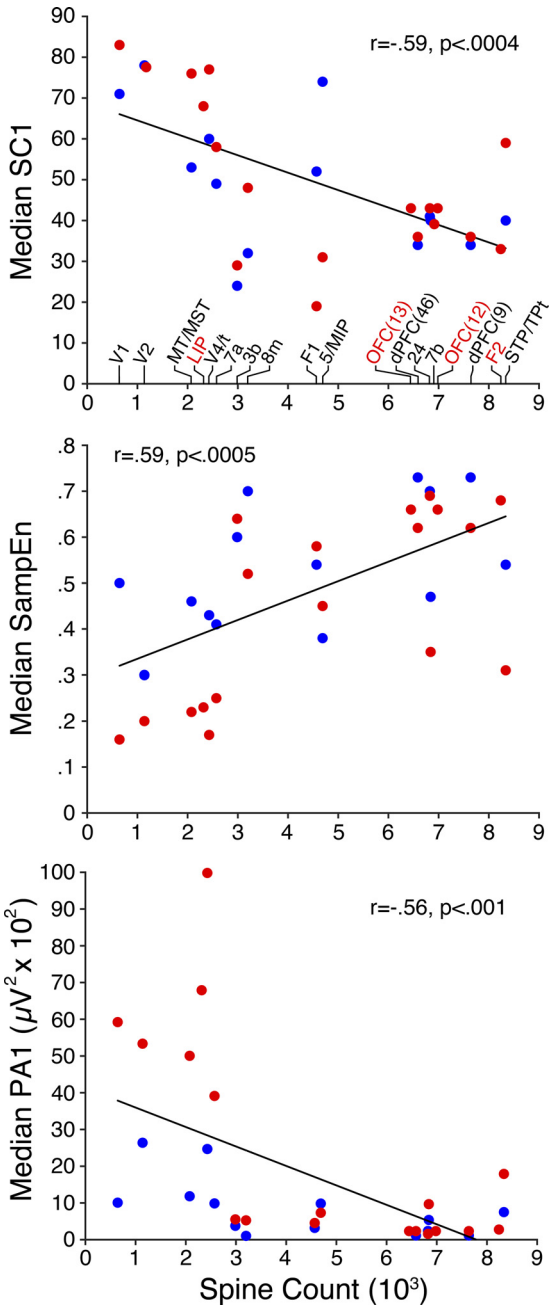

Figure 7. Scatter plots of the median values of spectral content in band 1 (SC1), sample entropy (SampEn) and peak amplitude in band 1 (PA1) vs. mean dendritic spine count on the basal dendrites of layer 3 pyramidal neurons for an overlapping set of 14 and 18 cortical areas in *monkey E* (blue) and *monkey L* (red). The correlation coefficients were calculated on the combined data from both monkeys. Spine counts along the *x*-axis are the same in all three plots and areal labels are shown above the *x*-axis in the top plot. Data for the areas labeled in black text were available for both monkeys while those labeled in red were available for *monkey L* only. Spine count data were taken from the reports of Elston and colleagues [Elston and Rosa (70–72); Elston and Rockland (73); Elston et al. (38, 74, 75)]. For some area groups (i.e., MT/MST, V4/t, 5/MIP, STP/TPt) spine data was obtained from just one area (i.e., MT, V4, 5, STP). For other area groups [i.e., orbital frontal cortex (orbFC) and dorsal prefrontal cortex (dPFC)], spine data was obtained from a subset of those areas (i.e., 12, 13, 9, and 46).

monkey E (Fig. 10, *C* and *D*) and *monkey L* (Fig. 10, *E* and *F*). Although the results differed between the two animals, several common findings were apparent in these plots. First, significant task-dependent increases and decreases in power occurred in at least one frequency band in every epoch of all areas in both monkeys, demonstrating widespread cortical involvement in the task. Second, the magnitude and incidence of the changes varied widely across areas and frequency bands. The spatial organization of the changes was most apparent in the incidence maps of Fig. 10, *D* and *F*. In *band 1*, prefrontal areas showed a task-dependent enhancement, particularly in *monkey L*, whereas suppression was common and robust in central, parietal, and occipital regions in both monkeys. In *band 2*, a complex combination of increases and decreases in power occurred across the cortical areas, making the spatial organization difficult to discern. Notably area V6A displayed a ramp-like enhancement in *band 2* in both monkeys, whereas area 8L showed a progressive suppression in *monkey L*. In *band 3*, the most apparent pattern was a combination of suppression in somatomotor, premotor, and prefrontal areas, and enhancement in parietal and extrastriate areas, particularly area V6A in *monkey L*. In *band 4* of *monkey L*, which was unique to this animal (see Fig. 3), a pronounced and ramp-like suppression of both the incidence and magnitude occurred throughout a broad region of cortex that included anterior parietal, somatomotor, premotor, and prefrontal areas. At the higher frequencies (*band 4* in *monkey E*, *band 5* in *monkey L*), the pattern of task-dependent changes differed between the two animals. In *monkey E*, there was a distinct enhancement in response to the sample stimuli in early visual cortex, most notably in foveal and perifoveal V1 (V1-SLVR). In *monkey L*, the changes in *band 5* showed a close spatial correspondence to the changes in *band 4*, but the responses were a mixture of increases and decreases of activity. Together, these results demonstrate widespread, task-dependent changes in the cortical LFP that span all the areas we recorded from. Moreover, the spatial organization of these changes varies with frequency and task epoch.

DISCUSSION

We made simultaneous measurements of intracortical neural activity in two monkeys performing a visual short-term memory task (50, 54) to investigate the spatial organization and task-dependence of the LFP across a significant fraction of the anatomically identified cortical areas in nonhuman primates (43). Analysis of the peak frequencies in the LFP power spectra revealed multiple narrow frequency bands in both animals. These distributions overlapped, but also differed in some key respects, demonstrating that the spectral composition of the cortical LFP can vary significantly between subjects and does not always fall neatly into classically defined canonical frequency bands. These results, along with differences in the recording locations and sample sizes, required us to confine the subsequent analyses to each monkey individually. We found that spatial maps and rank-ordered plots of two spectral parameters (SC, PA) revealed spatial gradients and large amplitude differences across the cortical map that differed markedly between frequency

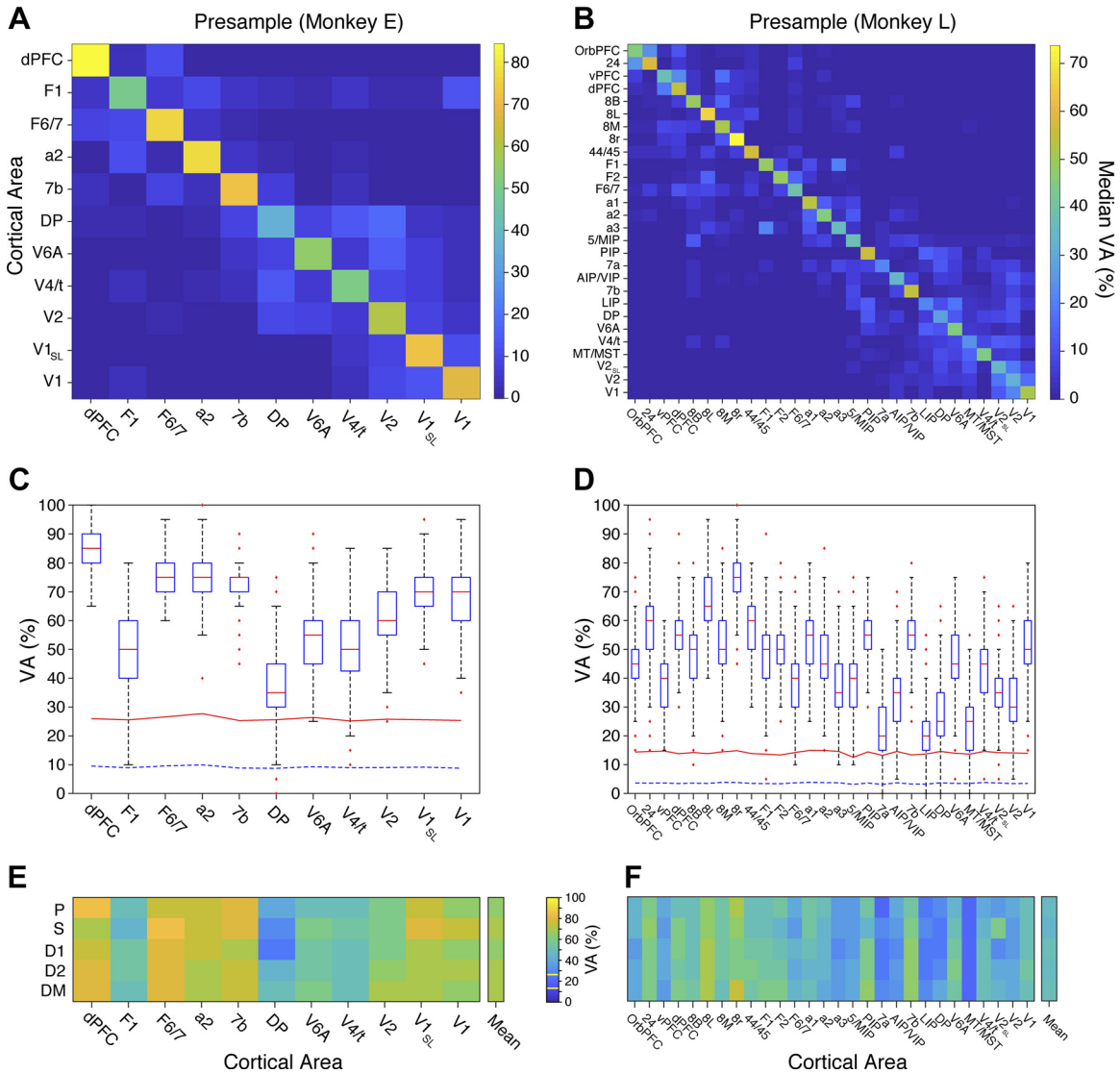

Figure 8. Results of the decoding analysis. Confusion matrices (*A* and *B*) and distributions of validation accuracies (*C* and *D*) for the presample epoch in *monkey E* (*A* and *C*) and *monkey L* (*B* and *D*). In each box plot the red line shows the median, the blue box displays the interquartile range, the whiskers show the 5th and 95th percentiles, and the red asterisks show outliers. The dashed blue line and solid red line in *C* and *D* show the mean and 99th percentile computed from the surrogate distributions. The plots in *E* and *F* show the median validation accuracies as a function of task epoch [Presample (P), Sample (S), Delay1 (D1), Delay2 (D2), and DelayM (DM)] for each area in *monkey E* and *monkey L*, respectively. The *upper* and *lower* yellow horizontal lines in the color-scale bar show the 99th percentile computed from the surrogate distributions for *monkeys E* and *L*, respectively. VA, validation accuracies. Cortical brain area abbreviations as per Ref. 43.

bands. These gradients were similar in the two monkeys, apart from *band 4* in *monkey L* that was absent in *monkey E*. Separate analysis of the temporal complexity of the LFP, using the measure of sample entropy (SampEn), revealed a similarly striking frontal to occipital gradient across the cortical map in both monkeys (Fig. 6). Together, these analyses demonstrate clear areal differences in the spectral and temporal properties of the LFP that exhibit multiple, distinct spatial gradients across the cortical map. These gradients are reminiscent of the earliest qualitative reports in humans and monkeys (28, 29, 77) and exhibit some similarities to a recent report in humans (31).

We also compared the spectral and temporal metrics of the LFP to the well documented gradients of synaptic spine counts on the basal dendrites of layer 3 pyramidal neurons (38, 70–75), which are closely correlated with areal hierarchy defined by interareal connections (43–45). This analysis revealed significant correlations between the synaptic spine counts and the low-frequency spectral components (SC1, PA1) and SampEn (Fig. 7) in both monkeys. Significant correlations were also present for SC and PA in *bands 2* and *3* in *monkey L*. These findings are particularly interesting, given the central role of temporal summation of dendritic synaptic currents in the genesis of the cortical LFP (25, 78, 79). However, these results were limited to spine counts on the basal dendrites of layer 3 pyramidal neurons because they have been exceptionally well studied. Much remains to be learned. We do not understand how the patterns of synaptic current give rise to the different spectral components of the LFP, nor how

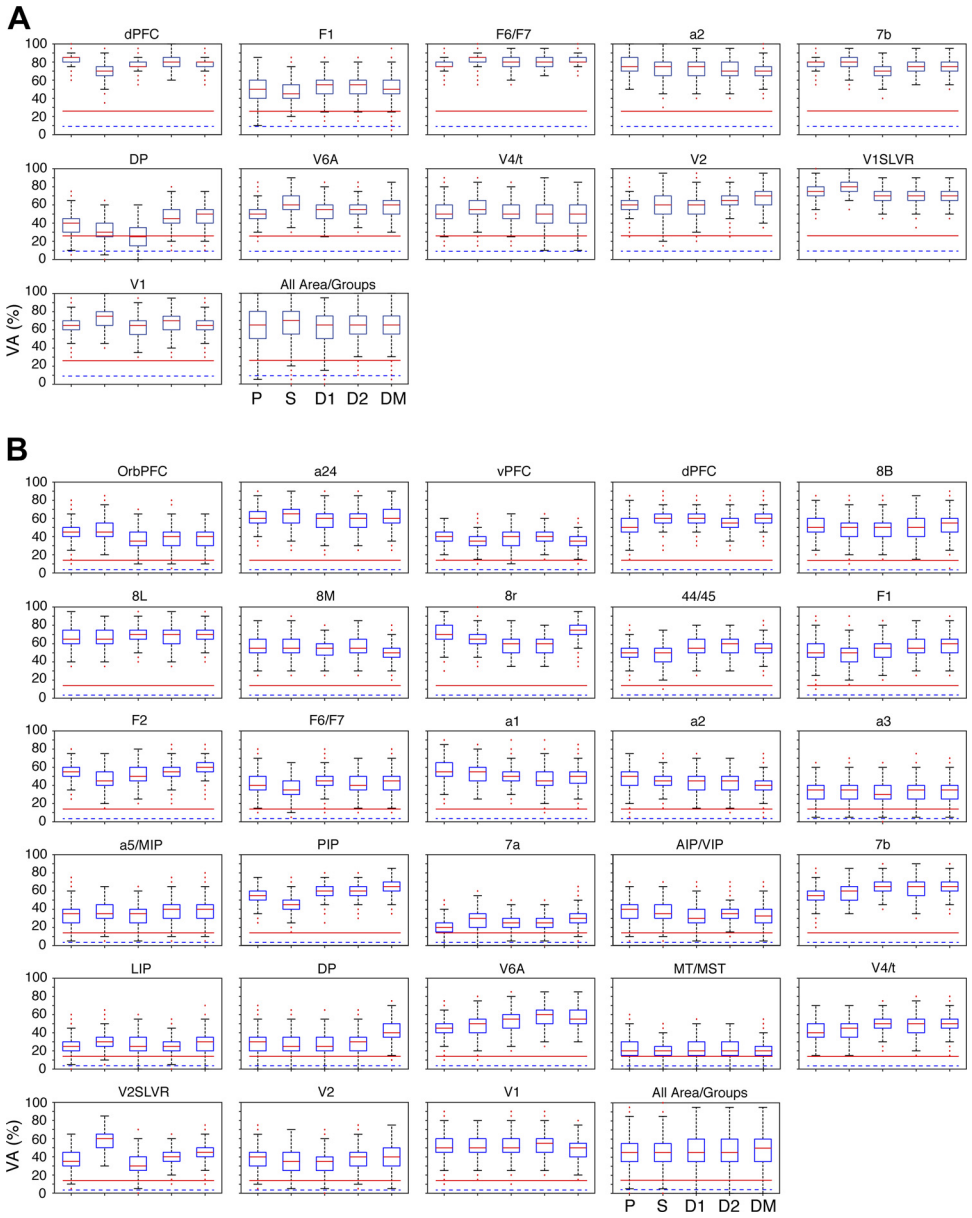

Figure 9. Distributions of validation accuracies (VA%) as a function of task epoch [Presample (P), Sample (S), Delay1 (D1), Delay2 (D2), and DelayM (DM)] for each area in *monkey E* (*A*) and *monkey L* (*B*). The bottom right plot in *A* and *B* shows the cumulative distributions of validation accuracies across all areas. In each box plot the red line shows the median, the blue box displays the interquartile range, the whiskers show the 5th and 95th percentiles, and the red asterisks show outliers. The dashed blue line and solid red line in each plot show the mean and 99th percentile computed from the surrogate distributions.

variations in synaptic organization might contribute to the gradients we observe. These findings are a new piece in a larger puzzle requiring further research.

Using the measures of spectral power and SampEn, we could reliably classify cortical areas, or small groups of areas, well above the 99% confidence limit derived from surrogate distributions that randomized areal assignment. The validation accuracy varied across epochs of the task in all areas. However, no single feature or frequency band incorporated in the analysis stood out as particularly informative, and validation accuracies exhibited a wide range in both monkeys. This suggested that variance in the feature distributions, or similarities in those distributions among nearby areas, could have led to degraded classification performance. We found evidence supporting both of these conjectures. Together, these analyses demonstrate widespread task-dependent changes in the LFP and show that the spectral features of the LFP display a considerable degree of overlap among adjacent areas, indicating that the LFP varies at a regional level incorporating multiple areas with related functional properties (30).

The decoding analysis, however, provided little or no information regarding the specific changes in spectral power that occur in each area during the task. We therefore calculated the magnitude and incidence of changes in power that occur in each area with respect to each frequency band and epoch of the task. This revealed the striking result that every area of the cortex we sampled in both monkeys displayed both significant increases and decreases in LFP power in multiple frequency bands and multiple epochs of the task. Thus, even a simple cognitive task, such as remembering a salient visual object for 1–2 s, evokes changes in power across widespread areas of the neocortex spanning, visual, parietal, somatomotor,

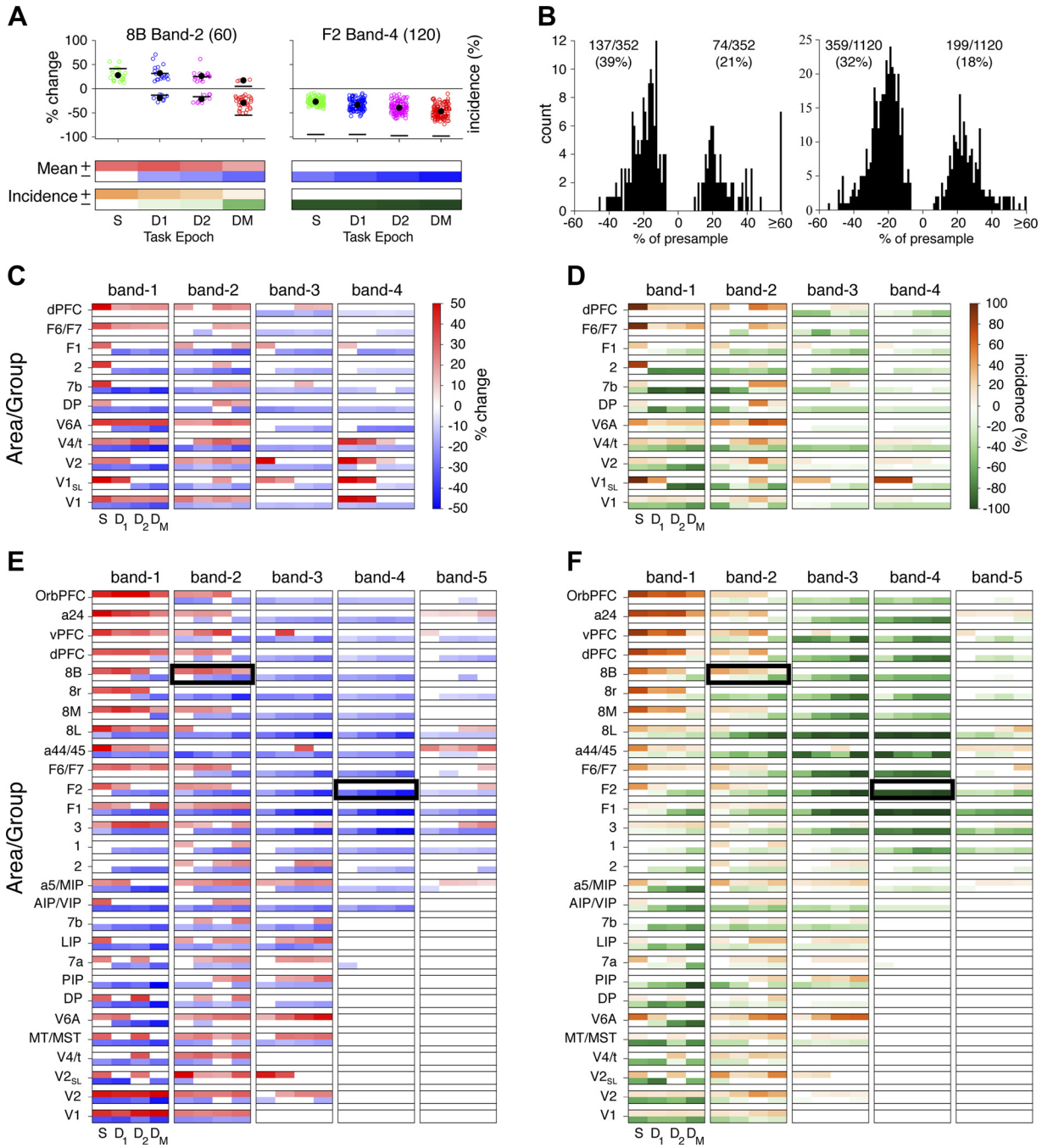

Figure 10. Task-dependent changes in local field potential (LFP) power as a function of task epoch, frequency band, and cortical area in *monkeys E* and *L*. *A*: example results for area 8B (*band 2*) and area F2 (*band 4*) in *monkey L*. The top plots show the distributions of significant changes in power across recording sites for each task epoch (S, sample; D1, delay1; D2, delay2; DM, delaym) as a percentage change relative to the presample epoch. The mean of each distribution is shown by the black filled circles. The incidence of significant values in each epoch is shown by the black horizontal lines. Recording counts are shown in parentheses. The mean change and the incidence values are color coded and displayed in the lower pair of plots for the two areas [mean change (blue/red), incidence (orange/green), see color scales in *C* and *D*]. *B*: histograms of the change in mean power, relative to the presample epoch, for all task epochs, frequency bands and cortical areas in *monkey E* (*left*) and *monkey L* (*right*). The ratios in each plot show the incidence (%) of significant decreases and increases in power. *C*–*F*: summaries of the significant changes in mean LFP power (*C* and *E*) and the incidence of those changes (*D* and *F*) as a function of task epoch (S, D1, D2, and DM), frequency band and cortical area for *monkey E* (*C* and *D*) and *monkey L* (*E* and *F*). The number of recordings in each area are given in Table 1. The black boxes in *E* and *F* indicate the data shown in the lower two pairs of plots in *A*.

premotor, and prefrontal areas. This result is consistent with our earlier findings of widespread, task-dependent changes in unit activity in the same data set (50). These findings are also consistent with a functional imaging study in humans demonstrating task-dependent changes in the blood oxygen level dependent (BOLD) signal in widespread regions of the brain during a simple visual attention task (57).

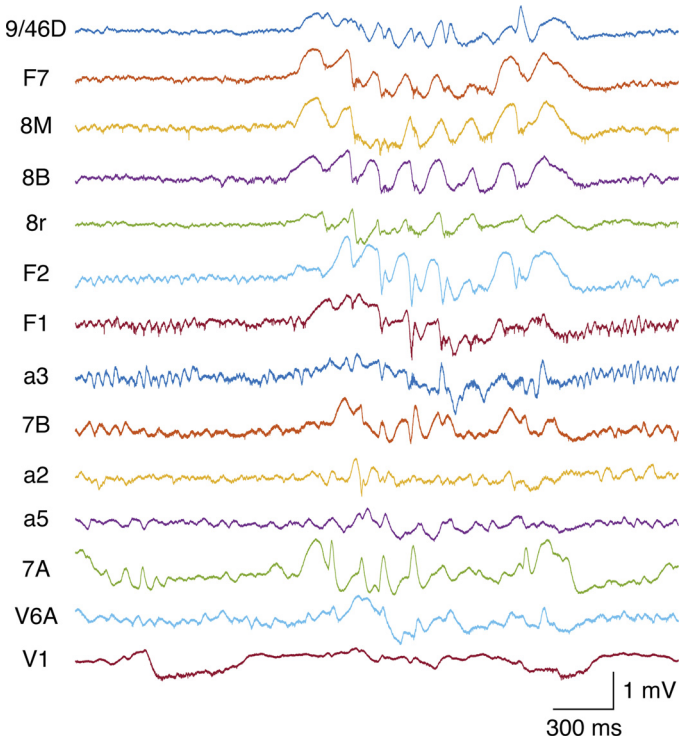

Figure 11. Plots of a 3-s segment of broadband raw data recorded during a period of rest with the room lights turned off in *monkey L*. The data is shown for the same channels on the same session as the plots in Fig. 2. A rapid-onset sleep spindle occurs halfway into the segment with high amplitude in prefrontal, premotor, and parietal areas.

Methodological Considerations

Our approach represents a significant advance over other methods such as electrocorticography (ECoG) that are limited to surface measurements with lower spatial resolution (80–82). However, the study also had several methodological limitations. First, we were unable to record from most ventral areas of the cortex, particularly in the temporal lobe. Second, the cortical areas we recorded from, and the size of the sample measured from each area, differed substantially between monkeys and between areas within each monkey. Part of this was due to an improvement in the methods used in *monkey L* (54). This sampling problem could have biased our results. For example, we obtained a large sample of recordings in area F2 in *monkey L*, but none in *monkey E* (Table 1). We made efforts to mitigate this problem by analyzing the data from each monkey separately and by subsampling the data from each area in each iteration of the decoding analysis. Third, although we were able to recover the areal location of each recording, we could not identify the cortical layer at each recording site. Given that the LFP is known to vary in amplitude and frequency across the cortical layers (9, 83, 84), the lack of layer information could have introduced significant variance or biased our results. Fourth, variations in arousal level are known to have pronounced influences on the spectral properties of the LFP (85), and these were clearly present in our data, particularly when the animals became drowsy or disinterested in the task (see Fig. 11). We attempted to reduce these effects by restricting our analysis to correct trials during periods of high performance on the task. Finally, the type of cognitive task, and the stimuli used in the task, are likely to have a significant influence on the properties of the LFP that depend on cortical area.

There were three other factors that could have affected our ability to discriminate differences in the LFP between cortical areas. First, because we used monopolar recording methods, volume conducted signals could have blurred the differences between areas. However, multiple lines of evidence indicate that the LFP is highly local (25, 79, 82, 84, 86, 87), suggesting that volume conduction has minimal effects on our data. Second, the reference channel in our recordings was tied to the large titanium chamber implanted on the animals (54). This provided a "quiet" reference potential by integrating signals from widespread areas of the skull. A separate analysis of the spectral coherence between simultaneously recorded LFPs revealed many instances of nonsignificant coherence at all frequencies (data not shown), suggesting that the reference signal is indeed quiet. Third, the 400-ms duration of the epoch-based spectral analysis, the multi-taper filtering of the power spectra, and the AC-coupling of our recording system, limited our ability to evaluate signals less than 4 Hz.

Finally, a further analytical issue concerns the spectral and temporal metrics we chose for characterizing the LFP. The SC and PA metrics provide overlapping and somewhat redundant information. However, they also made separate and useful contributions to the decoding analysis. In nearly all cortical areas, one feature performed significantly better than the other (see Supplemental Tables S1 and S2). This can occur, for example, when there is a big difference between areas in absolute power (PA), whereas the differences in relative power (SC) remain small. A related issue is present with SampEn, where the value of the metric likely reflects the relative power of low and high frequencies. In spite of this apparent redundancy, SampEn was informative in classifying cortical areas (see Supplemental Fig. S8). This metric also revealed a clear occipito-frontal gradient in both animals despite significant differences between animals in the distribution of peak frequencies shown in Fig. 3 and notable differences in the distribution of peak amplitudes shown in Fig. 5. Such a result would not be expected if this metric only reflected the relative magnitudes of low- and high-frequency power.

Frequency Differences

Outside of the low frequencies in *band 1*, we found several notable differences in the distribution of spectral peaks in the two monkeys. Signals with spectral peaks in *band 2* were widely distributed across the cortical areas in both monkeys but the frequencies were centered at 14 Hz in *monkey E* and 10 Hz in *monkey L*. Signals with spectral peaks in *band 3* were frontally distributed in both animals and centered at ~25 Hz in *monkey E* and ~20 Hz in *monkey L*. The narrow range of spectral peaks in *bands 4* and *5* of *monkey L* appeared to be completely absent in *monkey E*. Part of these differences may stem from the sampling problem discussed earlier. But perhaps the simplest explanation is that the occurrence and frequency distribution of narrow band oscillatory activity can differ widely between individuals and do not necessarily fall into the classically defined canonical frequency bands. This conclusion is supported by studies in

both monkeys and humans (13, 88–90), where the frequencies of narrow band oscillatory activity can differ significantly between individuals.

Regarding the higher frequency bands (*band 4* in *monkey E* and *bands 4* and *5* of *monkey L*), several results from this study were particularly noteworthy. First, the spectral peaks in *band 5* of *monkey L* (Figs. 2 and 3) co-occurred at twice the frequency of the high-amplitude narrow-band oscillations in *band 4*, suggesting a higher harmonic that is unlikely to reflect a distinct spectral component. Our supplemental analysis (Supplemental Figs. S4, S5, S6, and S7) confirmed this conjecture. Second, visually evoked γ-band (30–80 Hz) oscillations, characteristic of primary and early extrastriate areas of the visual cortex (69, 80, 86, 91, 92), were notably sparse and low amplitude in our data. This type of activity is known to depend on the use of appropriate visual stimuli that are tailored to the receptive field properties of the cortical neurons in those areas. Although we did observe clear instances of visually evoked γ-band oscillations in V1 and V2, particularly in *monkey E*, this was largely by chance, since we made no attempt to measure cellular receptive fields and adjust the sample stimuli to optimally activate the neurons at those recording sites. Third, we found limited evidence of elevated activity at the higher frequencies in either monkey during the delay period of the task (Fig. 10). In contrast, the oscillatory activity in this frequency range was nearly universally suppressed during the memory delay. This finding differs from several studies reporting elevated γ-band activity during the delay period of short-term memory tasks (10, 93–97), and argues against a role of γ-band activity as a general information carrier in the neocortex (98, 99).

Implications for Cortical Processing

Our findings also raise important questions regarding the concept of a hierarchy of intrinsic timescales across the cortex. The prevailing view, based on functional imaging and ECoG studies in humans (46, 47, 51) and single-unit studies in monkeys (49, 50, 52, 100), indicates that the intrinsic timescale, and temporal receptive window (47), of cortical areas gradually increase across the cortical hierarchy from sensory to association areas. Correspondence between the functional imaging and single-unit measures has also been recently implied in monkeys (101). Our findings, however, suggest an additional perspective. We find multiple, overlapping gradients of LFP power across cortical areas that display striking differences with respect to frequency (Figs. 4 and 5). Occipital-to-prefrontal gradients at low frequencies (*band 1*) transition to prefrontal-to-occipital gradients at higher frequencies (*bands 3–5*), whereas intermediate frequencies (*band 2*) display a unique gradient radiating from parietal and sensory-motor areas. If we consider 1/frequency as a simple measure of time scale, these gradients differ from and may be superimposed upon the hierarchical gradients established in previous studies. These findings may also account for the diversity of intrinsic time scales described in recent single-unit studies (52, 100). Our finding of widespread task dependence of LFP power further suggests that these gradients dynamically change with respect to cognitive task, attentional demands, and the types of sensory stimuli and motor actions (51).

Finally, our findings have important implications for the enduring view of cortical organization and function proposed by Mountcastle (102). In that classical monograph, Mountcastle proposed two fundamental tenets of cortical organization: The first of these, the unit module, synonymous with the cortical column, was proposed as a canonical circuit in which "... the processing function of neocortical modules is qualitatively similar in all neocortical regions ... without the appearance of qualitatively different modes of intrinsic organization." The striking differences we and many others find in the spectral and temporal properties of the LFP across cortical areas do in fact reveal "qualitatively distinct modes of intrinsic dynamics." When these results are combined with the well documented anatomical and functional gradients across the cortex (33–39, 42, 46–49, 103), a strictly canonical columnar model of neocortex (104) appears untenable. The second tenet was the concept of the distributed system, whereby "... complex function controlled or executed by the system is not localized to any one of its parts. The function is a property of the dynamic activity within the system: it resides in the system as such." Our finding of widespread task-dependent changes in spectral power that occur even for a simple cognitive task (57) reinforces the view of dynamic distributed processing as an integral feature of the central nervous system (105).

DATA AVAILABILITY

Data will be made available upon reasonable request.

SUPPLEMENTAL DATA

Supplementary Figs. S1–S9 and Supplemental Tables S1–S3: https://doi.org/10.6084/m9.figshare.25122929.

ACKNOWLEDGMENTS

We are grateful to Dr. Chris O'Rourke for her excellent veterinary care of the animals and assistance in this study. We thank Susan Krueger for her help in the behavioral training and daily care of the animals. We are grateful to Drs. Martin Vinck, Joachim Gross, and Pedro Maldonado for their helpful comments on earlier versions of the manuscript. We also thank Neuralynx (Neuralynx, Inc., Bozeman MT, USA) for providing the data acquisition system.

Present addresses: S. J. Hoffman, Dept. of Biomedical Engineering, University of Minnesota, Minneapolis, MN 55455, United States; N. M. Dotson, Salk Institute for Biological Studies, La Jolla, CA 92037, United States.

GRANTS

This work was supported by grants from National Institute of Neurological Disorders and Stroke (NINDS) under Grants R01 NS059312 and U19 NS107609, National Institute of Mental Health (NIMH) under Grant R01 MH081162, the McKnight Foundation Memory and Cognitive Disorders Award, an EPSCoR RII Track-2 award from the National Science Foundation (to C.M.G. and S.J.H.), and a T32 Neuroimaging training fellowship from NIH under Grant 1T32EB031512-01 (to S.J.H.).

DISCLOSURES

C.M.G. is affiliated with Gray Matter Research. None of the other authors has any conflicts of interest, financial or otherwise, to disclose.

AUTHOR CONTRIBUTIONS

S.J.H., N.M.D., and C.M.G. conceived and designed research; S.J.H., N.M.D., and C.M.G. performed experiments; S.J.H., N.M.D., V.L., and C.M.G. analyzed data; S.J.H., N.M.D., V.L., and C.M.G. interpreted results of experiments; S.J.H., N.M.D., V.L., and C.M.G. prepared figures; S.J.H., N.M.D., and C.M.G. drafted manuscript; S.J.H., N.M.D., and C.M.G. edited and revised manuscript; S.J.H., N.M.D., V.L., and C.M.G. approved final version of manuscript.

REFERENCES

1. **Bressler SL**, **Coppola R**, **Nakamura R.** Episodic multiregional cortical coherence at multiple frequencies during visual task performance. *Nature* 366: 153–156, 1993. doi:10.1038/366153a0.
2. **Tallon-Baudry C**, **Bertrand O**, **Fischer C.** Oscillatory synchrony between human extrastriate areas during visual short-term memory maintenance. *J Neurosci* 21: RC177, 2001. doi:10.1523/JNEUROSCI.21-20-j0008.2001.
3. **Jensen O**, **Gelfand J**, **Kounios J**, **Lisman JE.** Oscillations in the α band (9–12 Hz) increase with memory load during retention in a short-term memory task. *Cerebral Cortex* 12: 877–882, 2002. doi:10.1093/cercor/12.8.877.
4. **Brovelli A**, **Ding M**, **Ledberg A**, **Chen Y**, **Nakamura R**, **Bressler SL.** Beta oscillations in a large-scale sensorimotor cortical network: directional influences revealed by Granger causality. *Proc Natl Acad Sci USA* 101: 9849–9854, 2004. doi:10.1073/pnas.0308538101.
5. **Siegel M**, **Warden MR**, **Miller EK.** Phase-dependent neuronal coding of objects in short-term memory. *Proc Natl Acad Sci USA* 106: 21341–21346, 2009. doi:10.1073/pnas.0908193106.
6. **Liebe S**, **Hoerzer GM**, **Logothetis NK**, **Rainer G.** Theta coupling between V4 and prefrontal cortex predicts visual short-term memory performance. *Nat Neurosci* 15: 456–462, 2012. doi:10.1038/nn.3038.
7. **Salazar RF**, **Dotson NM**, **Bressler SL**, **Gray CM.** Content specific fronto-parietal synchronization during visual working memory. *Science* 338: 1097–1100, 2012. doi:10.1126/science.1224000.
8. **Dotson NM**, **Salazar RF**, **Gray CM.** Fronto-parietal correlation dynamics reveal interplay between integration and segregation during visual working memory. *J Neurosci* 34: 13600–13613, 2014. doi:10.1523/JNEUROSCI.1961-14.2014.
9. **Bastos AM**, **Loonis R**, **Kornblith S**, **Lundqvist M**, **Miller EK.** Laminar recordings in frontal cortex suggest distinct layers for maintenance and control of working memory. *Proc Natl Acad Sci USA* 115: 1117–1122, 2018. doi:10.1073/pnas.1710323115.
10. **Lundqvist M**, **Rose J**, **Herman P**, **Brincat SL**, **Buschman TJ**, **Miller EK.** Gamma and beta bursts underlie working memory. *Neuron* 90: 152–164, 2016. doi:10.1016/j.neuron.2016.02.028.
11. **Lobier M**, **Palva JM**, **Palva S.** High-α band synchronization across frontal, parietal and visual cortex mediates behavioral and neuronal effects of visuspatial attention. *Neuroimage* 165: 222–237, 2018. doi:10.1016/j.neuroimage.2017.10.044.
12. **Rezayat E**, **Dehaqani MA**, **Clark K**, **Bahmani Z**, **Moore T**, **Noudoost B.** Frontotemporal coordination predicts working memory performance and its local neural signatures. *Nat Commun* 12: 3811–3811, 2021. doi:10.1038/s41467-021-21151-1.
13. **Vezoli J**, **Vinck M**, **Bosman CA**, **Bastos AM**, **Lewis CM**, **Kennedy H**, **Fries P.** Brain rhythms define distinct interaction networks with differential dependence on anatomy. *Neuron* 109: 3862–3878.e5, 2021. doi:10.1016/j.neuron.2021.09.052.
14. **Singer W**, **Gray CM.** Visual feature integration and the temporal correlation hypothesis. *Annu Rev Neurosci* 18: 555–586, 1995. doi:10.1146/annurev.ne.18.030195.003011.
15. **Singer W.** Neuronal synchrony: a versatile code review for the definition of relations? *Neuron* 24: 49–65, 1999. doi:10.1016/s0896-6273(00)80821-1.
16. **Miller EK**, **Lundqvist M**, **Bastos AM.** Working memory 2.0. *Neuron* 100: 463–475, 2018. doi:10.1016/j.neuron.2018.09.023.
17. **Fries P.** A mechanism for cognitive dynamics: neuronal communication through neuronal coherence. *Trends Cogn Sci* 9: 474–480, 2005. doi:10.1016/j.tics.2005.08.011.
18. **Fries P.** Rhythms for cognition: communication through coherence. *Neuron* 88: 220–235, 2015. doi:10.1016/j.neuron.2015.09.034.
19. **Jensen O**, **Mazaheri A.** Shaping functional architecture by oscillatory α activity: gating by inhibition. *Front Hum Neurosci* 4: 186, 2010. doi:10.3389/fnhum.2010.00186.
20. **Hagan MA**, **Pesaran B.** Modulation of inhibitory communication coordinates looking and reaching. *Nature* 604: 708–713, 2022. doi:10.1038/s41586-022-04631-2.
21. **Singer W.** Consciousness and the binding problem. *Ann N Y Acad Sci* 929: 123–146, 2001. doi:10.1111/j.1749-6632.2001.tb05712.x.
22. **Gray CM.** Synchronous oscillations in neuronal systems: mechanisms and functions. *J Comput Neurosci* 1: 11–38, 1994. doi:10.1007/BF00962716.
23. **Buzsáki G**, **Draguhn A.** Neuronal oscillations in cortical networks. *Science* 304: 1926–1929, 2004. doi:10.1126/science.1099745.
24. **Wang XJ.** Neurophysiological and computational principles of cortical rhythms in cognition. *Physiol Rev* 90: 1195–1268, 2010. doi:10.1152/physrev.00035.2008.
25. **Pesaran B**, **Vinck M**, **Einevoll GT**, **Sirota A**, **Fries P**, **Siegel M**, **Truccolo W**, **Schroeder CE**, **Srinivasan R.** Investigating large-scale brain dynamics using field potential recordings: analysis and interpretation. *Nat Neurosci* 21: 903–919, 2018. doi:10.1038/s41593-018-0171-8.
26. **Berger H.** Über das elektroenkephalogramm des menschen. *Archiv f Psychiatrie* 87: 527–570, 1929. doi:10.1007/BF01797193.
27. **Jasper HH**, **Andrews HL.** Human brain rhythms. I. Recording techniques and preliminary results. *J Gen Psychol* 14: 98–126, 1936. doi:10.1080/00221309.1936.9713141.
28. **Jasper HH**, **Andrews HL.** Electro-encephalography. III. Normal differentiation of occipital and precentral regions in man. *Arch NeurPsych* 39: 96–115, 1938. doi:10.1001/archneurpsyc.1938.02270010106010.
29. **Jasper HH**, **Penfield W.** Electrocorticograms in man: effect of voluntary movement upon the electrical activity of the precentral gyrus. *Arch F Psychiatr U Z Neur* 183: 163–174, 1949. doi:10.1007/BF01062488.
30. **Keitel A**, **Gross J.** Individual human brain areas can be identified from their characteristic spectral activation fingerprints. *PLoS Biol* 14: e1002498, 2016. doi:10.1371/journal.pbio.1002498.
31. **Frauscher B**, **von Ellenrieder N**, **Zelmann R**, **Doležalová I**, **Minotti L**, **Olivier A**, **Hall J**, **Hoffmann D**, **Nguyen DK**, **Kahane P**, **Dubeau F**, **Gotman J.** Atlas of the normal intracranial electroencephalogram: neurophysiological awake activity in different cortical areas. *Brain* 141: 1130–1144, 2018. doi:10.1093/brain/awy035.
32. **Mahjoory K**, **Schoffelen JM**, **Keitel A**, **Gross J.** The frequency gradient of human resting-state brain oscillations follows cortical hierarchies. *eLife* 9: e53715, 2020. doi:10.7554/eLife.53715.
33. **Goulas A**, **Zilles K**, **Hilgetag CC.** Cortical gradients and laminar projections in mammals. *Trends Neurosci* 41: 775–788, 2018. doi:10.1016/j.tins.2018.06.003.
34. **Huntenburg JM**, **Bazin PL**, **Margulies DS.** Large-scale gradients in human cortical organization. *Trends Cogn Sci* 22: 21–31, 2018. doi:10.1016/j.tics.2017.11.002.
35. **Hilgetag CC**, **Beul SF**, **van Albada SJ**, **Goulas A.** An architectonic type principle integrates macrosopic corico-cortical connections with intrinsic cortical circuits of the primate brain. *Netw Neurosci* 3: 905–923, 2019. doi:10.1162/netn_a_00100.
36. **Wang XJ.** Macroscopic gradients of synaptic excitation and inhibition in the neocortex. *Nat Rev Neurosci* 21: 169–178, 2020. doi:10.1038/s41583-020-0262-x.
37. **Elston G.** Specialization of the neocortical pyramidal cell during primate evolution. In: *Evolution of Nervous Systems*, edited by Kaas JH, Preuss TM**.** Amsterdam: Elsevier, 2007, vol. 4, p. 191–242.
38. **Elston GN**, **Benavides-Piccione R**, **Elston A**, **Manger PR**, **DeFelipe J.** Pyramidal cells in prefrontal cortex of primates: marked differences in neuronal structure among species. *Front Neuroanat* 5: 2, 2011. doi:10.3389/fnana.2011.00002.
39. **Collins CE**, **Airey DC**, **Young NA**, **Leitch DB**, **Kaas JH.** Neuron densities vary across and within cortical areas in primates. *Proc Natl Acad Sci USA* 107: 15927–15932, 2010. doi:10.1073/pnas.1010356107.
40. **Beul SF**, **Barbas H**, **Hilgetag CC.** A predictive structural model of the primate connectome. *Sci Rep* 7: 43176, 2017. doi:10.1038/srep43176.
41. **Froudist-Walsh S**, **Bliss DP**, **Ding X**, **Rapan X**, **Niu M**, **Knoblauch K**, **Zilles K**, **Kennedy H**, **Palomero-Gallagher N**, **Wang XJ.** A dopamine gradient controls access to distributed working memory in the large-scale monkey cortex. *Neuron* 109: 3500–3520.e13, 2021. doi:10.1016/j.neuron.2021.08.024.

42. **Froudist-Walsh S**, **Xu T**, **Niu M**, **Rapan L**, **Zhao L**, **Margulies DS**, **Zilles K**, **Wang XJ**, **Palomero-Gallagher N.** Gradients of neurotransmitter receptor expression in the macaque cortex. *Nat Neurosci* 26: 1281–1294, 2023. doi:10.1038/s41593-023-01351-2.
43. **Markov NT**, **Ercsey-Ravasz MM**, **Ribeiro Gomes AR**, **Lamy C**, **Magrou L**, **Vezoli J**, **Misery P**, **Falchier A**, **Quilodran R**, **Gariel MA**, **Sallet J**, **Gamanut R**, **Huissoud C**, **Clavagnier S**, **Giroud P**, **Sappey-Marinier D**, **Barone P**, **Dehay C**, **Toroczkai Z**, **Knoblauch K**, **Van Essen DC**, **Kennedy H.** A weighted and directed interareal connectivity matrix for macaque cerebral cortex. *Cereb Cortex* 24: 17–36, 2014. doi:10.1093/cercor/bhs270.
44. **Markov NT**, **Vezoli J**, **Chameau P**, **Falchier A**, **Quilodran R**, **Huissoud C**, **Lamy C**, **Misery P**, **Giroud P**, **Ullman S**, **Barone P**, **Dehay C**, **Knoblauch K**, **Kennedy H.** Anatomy of hierarchy: feedforward and feedback pathways in macaque visual cortex. *J Comp Neurol* 522: 225–259, 2014. doi:10.1002/cne.23458.
45. **Chaudhuri R**, **Knoblauch K**, **Gariel MA**, **Kennedy H**, **Wang XJ.** A large-scale circuit mechanism for hierarchical dynamical processing in the primate cortex. *Neuron* 88: 419–431, 2015. doi:10.1016/j.neuron.2015.09.008.
46. **Hasson U**, **Yang E**, **Vallines I**, **Heeger DJ**, **Rubin N.** A hierarchy of temporal receptive windows in human cortex. *J Neurosci* 28: 2539–2550, 2008. doi:10.1523/JNEUROSCI.5487-07.2008.
47. **Hasson U**, **Chen J**, **Honey CJ.** Hierarchical process memory: memory as an integral component of information processing. *Trends Cogn Sci* 19: 304–313, 2015. doi:10.1016/j.tics.2015.04.006.
48. **Honey CJ**, **Thesen T**, **Donner TH**, **Silbert LJ**, **Carlson CE**, **Devinsky O**, **Doyle WK**, **Rubin N**, **Heeger DJ**, **Hasson U.** Slow cortical dynamics and the accumulation of information over long timescales. *Neuron* 76: 423–434, 2012 [Erratum in Neuron 76: 668, 2012]. doi:10.1016/j.neuron.2012.08.011.
49. **Murray JD**, **Bernacchia A**, **Freedman DJ**, **Romo R**, **Wallis JD**, **Cai X**, **Padoa-Schioppa C**, **Pasternak T**, **Seo H**, **Lee D**, **Wang X-J.** A hierarchy of intrinsic timescales across primate cortex. *Nat Neurosci* 17: 1661–1663, 2014. doi:10.1038/nn.3862.
50. **Dotson NM**, **Hoffman SJ**, **Goodell B**, **Gray CM.** Feature-based visual short-term memory is widely distributed and hierarchically organized. *Neuron* 99: 215–226.e4, 2018. doi:10.1016/j.neuron.2018.05.026.
51. **Gao R**, **van den Brink RL**, **Pfeffer T**, **Voytek B.** Neuronal timescales are functionally dynamic and shaped by cortical microarchitecture. *eLife* 9: e61277, 2020. doi:10.7554/eLife.61277.
52. **Spitmaan M**, **Seo H**, **Lee D**, **Soltani A.** Multiple timescales of neuronal dynamics and integration of task-relevant signals across cortex. *Proc Natl Acad Sci USA* 117: 22522–22531, 2020. doi:10.1073/pnas.2005993117.
53. **Dotson NM**, **Salazar RF**, **Goodell AB**, **Hoffman SJ**, **Gray CM.** Methods, caveats, and the future of large-scale microelectrode recordings in the non-human primate. *Front Syst Neurosci* 9: 149, 2015. doi:10.3389/fnsys.2015.00149.
54. **Dotson NM**, **Hoffman SJ**, **Goodell B**, **Gray CM.** A large-scale semi-chronic microdrive recording system for non-human primates. *Neuron* 96: 769–782.e2, 2017. doi:10.1016/j.neuron.2017.09.050.
55. **Richman JS**, **Moorman JR.** Physiological time-series analysis using approximate entropy and sample entropy. *Am J Physiol Heart Circ Physiol* 278: H2039–H2049, 2000. doi:10.1152/ajpheart.2000.278.6.H2039.
56. **Delgado-Bonal A**, **Marshak A.** Approximate entropy and sample entropy: a comprehensive tutorial. *Entropy* 21: 541, 2019. doi:10.3390/e21060541.
57. **Gonzalez-Castillo J**, **Saad ZS**, **Handwerker DA**, **Inati SJ**, **Brenowitz N**, **Bandettini PA.** Whole-bran, time-locked activation with simple tasks revealed using massive averaging and model-free analysis. *Proc Natl Acad Sci USA* 109: 5487–5492, 2012. doi:10.1073/pnas.1121049109.
58. **Asaad WF**, **Eskandar EN.** A flexible software tool for temporally precise behavioral control in matlab. *J Neurosci Methods* 174: 245–258, 2008. doi:10.1016/j.jneumeth.2008.07.014.
59. **Asaad WF**, **Eskandar EN.** Achieving behavioral control with millisecond resolution in a high-level programming environment. *J Neurosci Methods* 173: 235–240, 2008. doi:10.1016/j.jneumeth.2008.06.003.
60. **Yen SC**, **Baker J**, **Gray CM.** Heterogeneity in the responses of adjacent neurons to natural stimuli in cat striate cortex. *J Neurophysiol* 97: 1326–1341, 2007. doi:10.1152/jn.00747.2006.
61. **Oostenveld R**, **Fries P**, **Maris E**, **Schoffelen JM.** FieldTrip: open source software for advanced analysis of MEG, EEG, and invasive electrophysiological data. *Comput Intell Neurosci* 2011: 156869, 2011. doi:10.1155/2011/156869.
62. **Pincus SM.** Approximate entropy as a measure of system complexity. *Proc Natl Acad Sci USA* 88: 2297–2301, 1991. doi:10.1073/pnas.88.6.2297.
63. **Combrisson E**, **Jerbi K.** Exceeding chance level by chance: the caveat of theoretical chance levels in brain signal classification and statistical assessment of decoding accuracy. *J Neurosci Methods* 250: 126–136, 2015. doi:10.1016/j.jneumeth.2015.01.010.
64. **Aru J**, **Aru J**, **Priesemann V**, **Wibral M**, **Lana L**, **Pipa G**, **Singer W**, **Vicente R.** Untangling cross-frequency coupling in neuroscience. *Curr Opin Neurobiol* 31: 51–61, 2015. doi:10.1016/j.conb.2014.08.002.
65. **Lozano-Soldevilla D**, **Ter Huurne N**, **Oostenveld R.** Neuronal oscillations with non-sinusoidal morphology produce spurious phase-to-amplitude coupling and directionality. *Front Comput Neurosci* 10: 87, 2016. doi:10.3389/fncom.2016.00087.
66. **Gerber EM**, **Sadeh B**, **Ward A**, **Knight RT**, **Deouell LY.** Non-sinusoidal activity can produce cross-frequency coupling in cortical signals in the absence of functional interactions between neural sources. *PLoS One* 11: e0167351, 2016. doi:10.1371/journal.pone.0167351.
67. **Cole SR**, **van der Meij R**, **Peterson EJ**, **de Hemptinne C**, **Starrr PA**, **Voytek BJ.** Nonsinusoidal β oscillations reflect cortical pathophysiology in Parkinson's disease. *J Neurosci* 37: 4830–4840, 2017. doi:10.1523/JNEUROSCI.2208-16.2017.
68. **Schaworonkow N**, **Nikulin VV.** Spatial neuronal synchronization and the waveform of oscillations: implications for EEG and MEG. *PLoS Comput Biol* 15: e1007055, 2019. doi:10.1371/journal.pcbi.1007055.
69. **Friedman-Hill SR**, **Maldonado PE**, **Gray CM.** Dynamics of striate cortical activity in the alert macaque. I. Incidence and stimulus-dependence of gamma-band neuronal oscillations. *Cereb Cortex* 10: 1105–1116, 2000. doi:10.1093/cercor/10.11.1105.
70. **Elston GN**, **Rosa MG.** The occipitoparietal pathway of the macaque monkey: camparison of pyramidal cell morphology in layer III of functionally related cortical visual areas. *Cereb Cortex* 7: 432–452, 1997. doi:10.1093/cercor/7.5.432.
71. **Elston GN**, **Rosa MG.** Morphological variation of layer III pyramidal neurones in the occipitotemporal pathway of the macaque monkey visual cortex. *Cereb Cortex* 8: 278–294, 1998. doi:10.1093/cercor/8.3.278.
72. **Elston GN**, **Rosa MG.** Complex dendritic fields of pyramidal cells in the frontal eye field of the macaque monkey: comparison with parietal areas 7a and LIP. *Neuroreports* 9: 127–131, 1998b. doi:10.1097/00001756-199801050-00025.
73. **Elston GN**, **Rockland KS.** The pyramidal cell of the sensorimotor cortex of the macaque monkey: phenotypic variation. *Cereb Cortex* 12: 1071–1078, 2002. doi:10.1093/cercor/12.10.1071.
74. **Elston GN**, **Tweedale R**, **Rosa MP.** Cortical integration in the visual system of the macaque monkey: largescale morphological differences of pyramidal neurones in the occipital, parietal and temporal lobes. *Proc Biol Sci* 266: 1367–1374, 1999. doi:10.1098/rspb.1999.0789.
75. **Elston GN**, **Benavides-Piccione R**, **DeFelipe J.** A study of pyramidal cell structure in the cingulate cortex of the macaque monkey with comparative notes on inferotemporal and primary visual cortex. *Cereb Cortex* 15: 64–73, 2005. doi:10.1093/cercor/bhh109.
76. **Dreyfus G**, **Guyon I.** Assessment methods. In: *Feature Extraction: Foundations and Applications,* edited by Guyon I, Gunn S, Nikravesh M, Zadeh L. Cham, Switzerland: Springer, 2006, p. 65–88.
77. **Garvin JS**, **Amador LV.** Electrocorticograms of the cytoarchitectural areas of *Macaca Mulatta*. *J Neurophysiol* 12: 425–433, 1949. doi:10.1152/jn.1949.12.6.425.
78. **Lindén H**, **Tetzlaff T**, **Potjans TC**, **Pettersen KH**, **Grün S**, **Diesmann M**, **Einevoll GT.** Modeling the spatial reach of the LFP. *Neuron* 72: 859–872, 2011. doi:10.1016/j.neuron.2011.11.006.
79. **Einevoll GT**, **Kayser C**, **Logothetis NK**, **Panzeri S.** Modeling and analysis of local field potentials for studying the function of cortical circuits. *Nat Rev Neurosci* 14: 770–785, 2013. doi:10.1038/nrn3599.
80. **Bosman CA**, **Schoffelen JM**, **Brunet N**, **Oostenveld R**, **Bastos AM**, **Womelsdorf T**, **Rubehn B**, **Stieglitz T**, **De Weerd P**, **Fries P.** Attentional stimulus selection through selective synchronization between monkey visual areas. *Neuron* 75: 875–888, 2012. doi:10.1016/j.neuron.2012.06.037.

81. **Bastos AM**, **Vezoli J**, **Bosman CA**, **Schoffelen JM**, **Oostenveld R**, **Dowdall JR**, **De Weerd P**, **Kennedy H**, **Fries P.** Visual areas exert feedforward and feedback influences through distinct frequency channels. *Neuron* 85: 390–401, 2015. doi:10.1016/j.neuron.2014.12.018.
82. **Dubey A**, **Ray S.** Cortical electrocorticogram (ECoG) is a local signal. *J Neurosci* 39: 4299–4311, 2019. doi:10.1523/JNEUROSCI.2917-18.2019.
83. **Murthy VN**, **Fetz EE.** Oscillatory activity in sensorimotor cortex of awake monkeys: synchronization of local field potentials and relation to behavior. *J Neurophysiol* 76: 3949–3967, 1996. doi:10.1152/jn.1996.76.6.3949.
84. **Spaak E**, **Bonnefond M**, **Maier A**, **Leopold DA**, **Jensen O.** Layer-specific entrainment of gamma-band neural activity by the α rhythm in monkey visual cortex. *Curr Biol* 22: 2313–2318, 2012. doi:10.1016/j.cub.2012.10.020.
85. **Magoun HW.** Brain mechanisms for wakefulness. *Br J Anaesth* 33: 183–193, 1961. doi:10.1093/bja/33.4.183.
86. **Gray CM**, **Singer W.** Stimulus-specific neuronal oscillations in orientation columns of cat visual cortex. *Proc Natl Acad Sci USA* 86: 1698–1702, 1989. doi:10.1073/pnas.86.5.1698.
87. **Katzner S**, **Nauhaus I**, **Benucci A**, **Bonin V**, **Ringach DL**, **Carandini M.** Local origin of field potentials in visual cortex. *Neuron* 61: 35–41, 2009. doi:10.1016/j.neuron.2008.11.016.
88. **Kilavik BE**, **Ponce-Alvarez A**, **Trachel R**, **Confais J**, **Takerkart S**, **Riehle A.** Context-related frequency modulations of macaque motor cortical LFP β oscillations. *Cereb Cortex* 22: 2148–2159, 2012. doi:10.1093/cercor/bhr299.
89. **van Pelt S**, **Boomsma DI**, **Fries P.** Magnetoencephalography in twins reveals a strong genetic determination of the peak frequency of visually induced γ-band synchronization. *J Neurosci* 32: 3388–3392, 2012. doi:10.1523/JNEUROSCI.5592-11.2012.
90. **Confais J**, **Malfait N**, **Brochier T**, **Riehle A**, **Kilavik BE.** Is there an intrinsic relationship between LFP β oscillation amplitude and firing rate of individual neurons in macaque motor cortex? *Cereb Cortex Commun* 1: tgaa017, 2020. doi:10.1093/texcom/tgaa017.
91. **Fries P**, **Reynolds JH**, **Rorie AE**, **Desimone R.** Modulation of oscillatory neuronal synchronization by selective visual attention. *Science* 291: 1560–1563, 2001. doi:10.1126/science.1055465.
92. **Bartoli E**, **Bosking W**, **Chen Y**, **Li Y**, **Sheth SA**, **Beauchamp MS**, **Yoshor D**, **Foster BL.** Functionally distinct γ range activity revealed by stimulus tuning in human visual cortex. *Curr Biol* 29: 3345–3358. e7, 2019. doi:10.1016/j.cub.2019.08.004.
93. **Pesaran B**, **Pezaris JS**, **Sahani M**, **Mitra PP**, **Andersen RA.** Temporal structure in neuronal activity during working memory in macaque parietal cortex. *Nat Neurosci* 5: 805–811, 2002. doi:10.1038/nn890.
94. **Howard MW**, **Rizzuto DS**, **Caplan JB**, **Madsen JR**, **Lisman J**, **Aschenbrenner-Scheibe R**, **Schulze-Bonhage A**, **Kahana MJ.** Gamma oscillations correlate with working memory load in humans. *Cereb Cortex* 13: 1369–1374, 2003. doi:10.1093/cercor/bhg084.
95. **Meltzer JA**, **Zaveri HP**, **Goncharova II**, **Distasio MM**, **Papademetris X**, **Spencer SS**, **Spencer DD**, **Constable RT.** Effects of working memory load on oscillatory power in human intracranial EEG. *Cereb Cortex* 18: 1843–1855, 2008. doi:10.1093/cercor/bhm213.
96. **Roux F**, **Wibral M**, **Mohr HM**, **Singer W**, **Uhlhaas PJ.** Gamma-band activity in human prefrontal cortex codes for the number of relevant items maintained in working memory. *J Neurosci* 32: 12411–12420, 2012. doi:10.1523/JNEUROSCI.0421-12.2012.
97. **Honkanen R**, **Rouhinen S**, **Wang SH**, **Palva JM**, **Palva S.** Gamma oscillations underlie the maintenance of feature-specific information and the contents of visual working memory. *Cereb Cortex* 25: 3788–3801, 2015. doi:10.1093/cercor/bhu263.
98. **Fries P.** Neuronal γ-band synchronization as a fundamental process in cortical computation. *Annu Rev Neurosci* 32: 209–224, 2009. doi:10.1146/annurev.neuro.051508.135603.
99. **Başar E.** A review of γ oscillations in healthy subjects and in cognitive impairment. *Int J Psychophysiol* 90: 99–117, 2013. doi:10.1016/j.ijpsycho.2013.07.005.
100. **Cavanagh SE**, **Hunt LT**, **Kennerley SW.** A diversity of intrinsic timescales underlie neural computations. *Front Neural Circuits* 14: 615626, 2020. doi:10.3389/fncir.2020.615626.
101. **Manea A**, **Zilverstand A**, **Ugurbil K**, **Heilbronner S**, **Zimmermann J.** Intrinsic timescales as an organizational principle of neural processing across the whole rhesus macaque brain. *eLife* 11: e75540, 2022. doi:10.7554/eLife.75540.
102. **Mountcastle VB.** An organizing principle for cerebral function: the unit module and the distributed system. In: *The Neurosciences: Fourth Study Program*, edited by Schmitt FO, Worden FG**.** Cambridge: MIT Press, 1979, p. 21–42.
103. **Li S**, **Wang XJ.** Hierarchical timescales in the neocortex: mathematical mechanism and biological insights. *Proc Natl Acad Sci USA* 119: e2110274119, 2022. doi:10.1073/pnas.2110274119.
104. **Hawkins J.** *A Thousand Brains: A New Theory of Intelligence*. New York: Basic Books, 2021.
105. **Tognoli E**, **Kelso JA.** The metastable brain. *Neuron* 81: 35–48, 2014. doi:10.1016/j.neuron.2013.12.022.